Geomorphology 337 (2019) 111–133

Contents lists available at ScienceDirect

Geomorphology

journal homepage: www.elsevier.com/locate/geomorph

Glacier dynamics during a phase of Late Quaternary warming in Patagonia reconstructed from sediment-landform associations

Julian R.V. Martin *, Bethan J. Davies, Varyl R. Thorndycraft

Centre for Quaternary Research, Department of Geography, Royal Holloway University of London, Egham, Surrey TW20 0EX, UK

ARTICLE INFO

Article history:
Received 28 November 2018
Received in revised form 4 March 2019
Accepted 4 March 2019
Available online 01 April 2019

Keywords:
Patagonian Ice Sheet
Glacial sedimentology
Glacial landsystems
Palaeolakes

ABSTRACT

The geomorphological record in glaciated landscapes can provide important information for the study of the response of glaciers to rapid climate change. This study presents a new reconstruction of the glacial history of the northern Monte San Lorenzo ice cap, southern South America, during a period of accelerated warming and deglaciation following the Antarctic Cold Reversal (14.5–12.8 ka). We present a detailed geomorphological map of the valleys to the north of Monte San Lorenzo. Sediment-landform assemblages identified include lateral and terminal moraine ridges, flutes, deltas, ice-contact fans, palaeoshorelines, kame terraces and outwash plains. We map 14 primary ice-limits, 7 of which are newly identified, and 7 of which are from previous studies, mapped here in greater detail. We devise landsystem models to formalise and document spatial and temporal changes in glacial processes and environments. Our new geomorphological mapping and landsystem reconstructions provide an important insight into the response of temperate Patagonian glaciers to rapidly-warming climate.

© 2019 Published by Elsevier B.V.

1. Introduction

Atmospheric cooling during the Antarctic Cold Reversal (ACR, 14.5–12.8 ka) resulted in glacier readvance in the Southern Hemisphere mid-latitudes as shown by cosmogenic nuclide dating from moraine systems in Patagonia (García et al., 2012; Nimick et al., 2016; Darvill et al., 2017; Davies et al., 2018; Sagredo et al., 2018) and New Zealand (Putnam et al., 2010). In central Patagonia, the outlet glaciers of the Northern Patagonia Icefield had receded back to the valleys of the Andean Cordillera by the time of the ACR readvance and many were terminating in large proglacial lakes (Davies et al., 2018; Thorndycraft et al., 2019). Antarctic ice core records, such as the WAIS Divide, show that the ACR in the Southern Hemisphere high latitudes was followed by ca. 4000 years of warming from ca. 13.0–9.0 ka, with rapid warming of 2 °C between ca. 13.0 and 12.0 ka (Buizert et al., 2015). The geomorphic setting and evolution of Patagonian valley glaciers during post-ACR warming make them an interesting analogue for understanding present-day glacial dynamics in rapidly-warming, temperate climatic settings. During this period and the subsequent Holocene, glacier recession and punctuated readvances left behind discrete geomorphological features, revealing past glaciolacustrine, fjord-terminating and land-terminating glacier landsystems (Glasser et al., 2009; Davies et al., 2018). Little work has been done to investigate the evolution and interaction of these landsystems, in particular those associated with the smaller ice caps located in the Cordillera east of the Patagonian icefields (72–73°W). These localities provide opportunities for elucidating the roles of climatic, topographic and glaciolacustrine controls on the evolution of late Quaternary glaciated valleys found in Patagonia (Glasser et al., 2009). Morphological and sedimentological data from low-altitude, shallowly-sloping, steep-sided interlinked valleys, are currently limited and furthermore subsequent paraglacial modification has also received little attention in Patagonia.

Herein we establish sediment-landform assemblages and use a landsystems framework to examine the sedimentology and geomorphology of landforms in valleys to the north of the Monte San Lorenzo ice cap in Chile, formed during a period of overall atmospheric warming. These valleys represent contrasting styles of landsystems, including glaciolacustrine, land-terminating and glaciofluvial, but with significant paraglacial modification, and juxtaposed with small-scale mountain glaciers. Comparing these different landsystems will provide a template for understanding the roles different processes play in landscape evolution and modification in Patagonia. We aim to elucidate the nature and relative timing of changes in glacial environments, dynamics and processes since the ACR in order to assess the role of topography and ice-dammed lakes on palaeoglacier dynamics. Our objectives are: 1) to determine sediment-landform assemblages across a spectrum of palaeoglacial and glacial environments; 2) generate landsystems'

* Corresponding author.
E-mail address: julian.martin.2016@live.rhul.ac.uk (J.R.V. Martin).

https://doi.org/10.1016/j.geomorph.2019.03.007
0169-555X/© 2019 Published by Elsevier B.V.

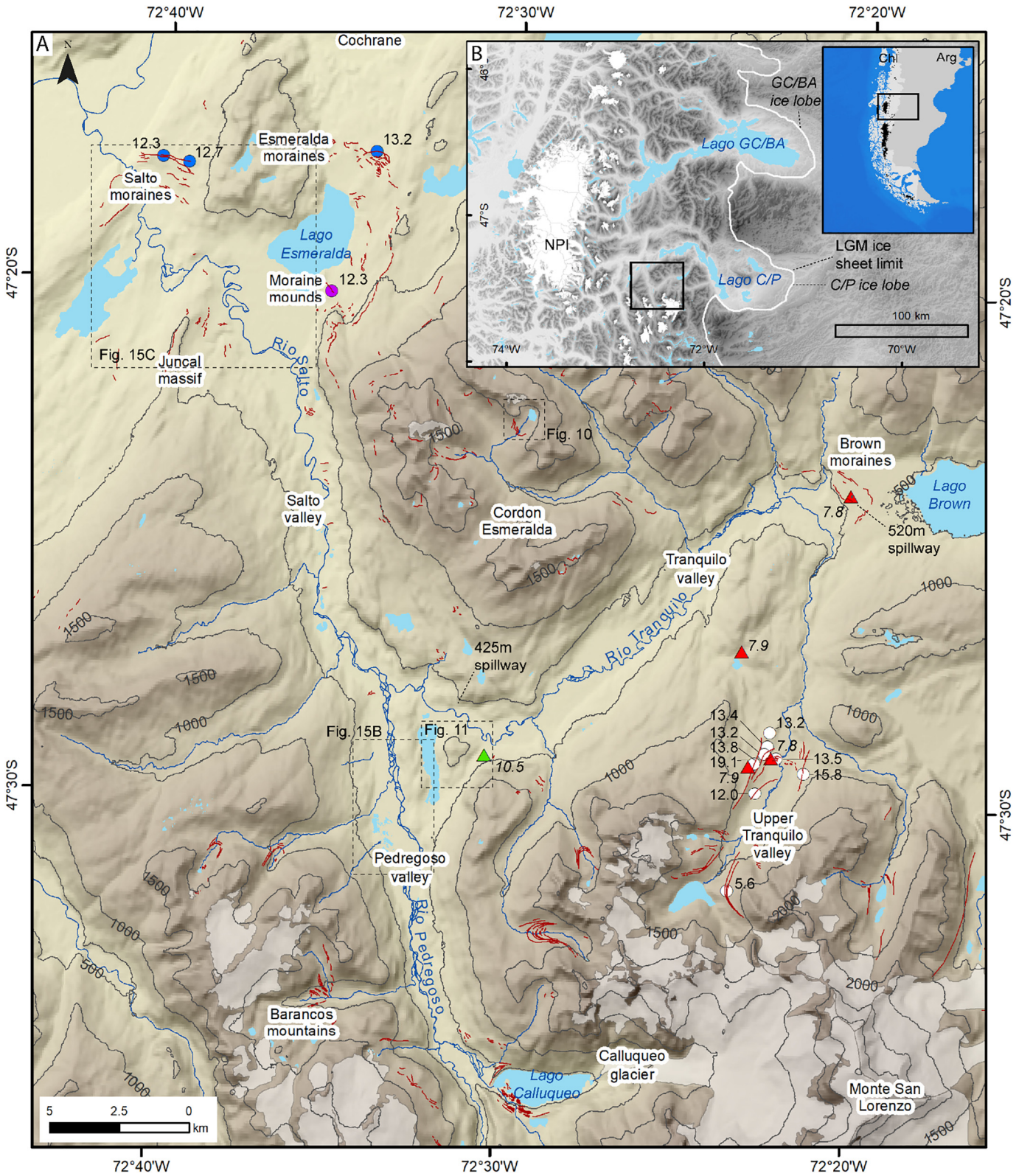
72°40'W
72°30'W
72°20'W
47°20'S
47°30'S
A
N
Cochrane
B
GC/BA ice lobe
Lago GC/BA
NPI
Lago C/P
LGM ice sheet limit
C/P ice lobe
100 km
Chl
Arg
48°
47°S
74°W
72°W
70°W
12.3
12.7
Esmeralda moraines
13.2
Salto moraines
Lago Esmeralda
Moraine mounds
12.3
Fig. 15C
Juncal massif
Río Salto
Fig. 10
Salto valley
Cordon Esmeralda
Brown moraines
Lago Brown
7.8
520m spillway
Tranquilo valley
Río Tranquilo
425m spillway
7.9
Fig. 15B
Fig. 11
10.5
13.4
13.2
13.8
19.1
7.9
12.0
13.2
7.8
13.5
15.8
Upper Tranquilo valley
5.6
Pedregoso valley
Río Pedregoso
Barancos mountains
Calluqueo glacier
Lago Calluqueo
Monte San Lorenzo
1500
1000
500
2000
5
2.5
0
km
Glaciers
Lake
River
Moraine ridge
14C and tephra sites and ages
Stern et al., 2016
Gardeweg and Sellés 2013
Cosmogenic nuclide sample sites and ages
Davies et al., 2018
Sagredo et al., 2018
Glasser et al., 2012

models explaining the processes of sediment-landform generation in central Patagonia; and 3) elucidate the influence of ice-dammed lakes and other controls on palaeoglacier dynamics.

2. Study area

Monte San Lorenzo (47°35′S, 72°18′W) is an isolated granodioritic to granitic massif (Ramos et al., 1982) on the eastern flank of the Andean range, located ca. 70 km east of the southern point of the Northern Patagonian Icefield (NPI) (Fig. 1). It experiences a temperate climate with mean annual air temperature of 8.4 °C and average annual precipitation of 750 mm w.e. (Direccion Meteologica de Chile, 2001) recorded at the nearest meteorological station in the town of Cochrane 40 km to the north (47°14′S, 72°33′W; 182 m asl).

At the LGM, ice from glaciers on the western and northern flanks of Monte San Lorenzo discharged into the Salto and Tranquilo valleys, coalescing with the Cochrane/Pueyrredón (CP) outlet lobe from the NPI (Wenzens, 2002). The CP and General Carrera/Buenos Aires (GCBA) outlet lobes reached the Argentinian lowlands (Fig. 1B) forming large moraine sequences (Caldenius, 1932; Mercer, 1976; Douglass et al., 2006; Hein et al., 2010; Bendle et al., 2017a; Mendelova et al., 2017). Upon ice recession, large ice-dammed lakes formed in the Lago GCBA and Lago CP valleys, draining to the Atlantic (Turner et al., 2005; Bell, 2008; García et al., 2014). Subsequent punctuated drops in lake level occurred as lower elevation drainage pathways opened and drainage switched to the Pacific (Turner et al., 2005; Bell, 2008, 2009; Hein et al., 2010; Bourgois et al., 2016; Glasser et al., 2016; Davies et al., 2018; Thorndycraft et al., 2019). During this period, the large unified palaeolake "Lago Chelenko" occupied the Cochrane and Lago GCBA valleys at 340–350 m asl, dammed by Pared Norte Glacier to the east (Davies et al., 2018; Thorndycraft et al., 2019). Ice discharging from Monte San Lorenzo and the eastern Barrancos Mountains contributed to large glaciers in the Salto and Tranquilo valleys (Davies et al., 2018). Ice in the Salto valley coalesced to terminate in Lago Chelenko, forming the ACR Esmeralda moraines at 13.2 ± 0.2 ka (Davies et al., 2018; Thorndycraft et al., 2019) (this and dates that follow are recalculated as per protocols in Section 3). Recession of ice formed a series of inset moraines, including the "Moraine Mounds" (Fig. 1) dated to ca. 12.3 ± 0.4 ka (Glasser et al., 2012). A radiocarbon date below the H1 tephra layer at the Tranquilo-Salto confluence (Gardeweg and Sellés, 2013) is recalculated to 10.5 ± 0.1 cal ka BP providing a minimum age for ice-free conditions at the Tranquilo-Salto confluence. The H1 tephra has been found in bog cores in the Tranquilo and upper Tranquilo valleys with an average age across localities of 7.9 cal ka BP (Stern et al., 2016) (Fig. 1).

In the upper Tranquilo valley, Tranquilo Glacier formed moraines prior to the ACR with a maximum age limit of 19.1 ± 0.8 ka. A cluster of moraines in the upper Tranquilo valley also date to the ACR at 13.8 ± 0.1 ka (Sagredo et al., 2018). Subsequent moraine sets in the upper Tranquilo valley have been dated to between 13.5 and 13.2 ka, and 12.0 ± 0.3 ka (Sagredo et al., 2018). Finally, a mid-Holocene moraine in the upper Tranquilo valley is dated to 5.6 ± 0.1 ka (Sagredo et al., 2018).

Today, small-scale glaciers occupy high ground on Cordon Esmeralda (Fig. 1). Monte San Lorenzo supports a small ice cap with an area of ca. 139 km^2, with the largest outlet glacier, Calluqueo Glacier, descending down to 520 m asl (Falaschi et al., 2013). There is asymmetry in the snowline attributed to regional precipitation gradients: 1700–1750 m asl in the wetter western sectors and 1800 m asl in the drier eastern sectors (Falaschi et al., 2013). The glacial, glaciolacustrine, glaciofluvial and paraglacial landforms and deposits in the Salto, Tranquilo and Pedregoso valleys formed through the late Pleistocene and Holocene make up the basis for our sediment-landform study.

3. Methods

The Salto, Tranquilo and Pedregoso valleys were mapped and digitised in ArcMap 10.3 at 1:5000 scale using 1 m resolution DigitalGlobe imagery, part of the Esri™ World Imagery. Google Earth Pro (DigitalGlobe imagery) was used in conjunction to this, alongside Google Earth's digital elevation model to view landforms from an oblique perspective, aiding identification. Additional elevation data were taken from an ASTER G-DEM (20 m vertical and 30 m horizontal resolution, 95% confidence; cf. ASTER GDEM Validation Team, 2011). Field mapping (Nov-Dec 2016 and Dec 2017) was used to ground-truth remotely sensed mapping and improve landform identification and mapping detail. Roadside cuttings along the Salto and Tranquilo valleys provided sediment exposures for landforms. Landforms in the field were mapped using handheld GPS with a documented accuracy of ±10 m.

Well established criteria for landform identification, both by remote sensing and in the field, were used (Glasser et al., 2005, 2008; Bendle et al., 2017b; Darvill et al., 2017; Chandler et al., 2018) and adapted to account for the specific characteristics of landforms found in the study area (Table 1). Moraine ridges were grouped into 'sets' based upon their relative position within a valley to delineate a period of ice-marginal stability. Frontal and lateral moraines which could be traced to one another, or lateral moraines at the same altitude on opposite valley sides, were grouped into the same set. We group landforms into 5 sediment-landform associations that we outline in Sections 4.2 to 4.6: ice-marginal, subglacial, glaciolacustrine, glaciofluvial and paraglacial.

Sedimentological and stratigraphical studies were undertaken at exposures through landforms (road cuttings and quarry sites) along the Salto and Tranquilo valleys using standard procedures (Evans and Benn, 2004). Clast morphology data (shape and roundness) were collected from representative facies, following Benn (2004), to investigate transportation and erosion histories. Shape data were plotted on a general shape ternary diagram (Sneed and Folk, 1958; Benn and Ballantyne, 1993) and from this C_{40} indices (Benn and Ballantyne, 1993) were calculated. Roundness data were plotted as histograms and analysed statistically using RA and RWR indices (Evans and Benn, 2004). We use RWR indices alongside RA to mitigate for the influence of glaciofluvial reworking on the effectiveness of the RA index to distinguish transport pathways (Evans et al., 2010, 2013; Lukas et al., 2013). Cosmogenic nuclide surface exposure ages were recalculated (Fig. 1) using version 3 of the online exposure age calculator formerly known as the CRONUS-Earth online exposure age calculator (Balco et al., 2008) with a regional Patagonian production rate calculated from the Kaplan et al. (2011) calibration data set. Ages presented assume a 0 mm/kyr erosion rate, use the time dependent Lm scaling method (Lal, 1991; Stone, 2000) and are calculated as uncertainty weighted means (UWM) of multiple samples taken over single moraine ridges/contemporaneous sets, rounded to the nearest 0.1 ka.

4. Results

4.1. Landform inventory of the northern Monte San Lorenzo sector

Combining remote sensing and field mapping, including within forested areas, has allowed us to map in greater detail the landforms of the study area. Subsequently we have identified previously unmapped landforms and increased the extent and detail of those mapped in previous studies in this region that have relied on satellite imagery (Glasser and Jansson, 2005, 2008; Turner et al., 2005; Glasser et al., 2009, 2012; Bendle et al., 2017b; Davies et al., 2018). The landform inventory for the northern Monte San Lorenzo sector contains 19 primary landform types (Fig. 2) which includes 1083 individual moraine ridges mapped alongside rivers, lakes, outcropping bedrock and bedrock

Fig. 1. (A) Map of the study area north of the Monte San Lorenzo Icecap including sites and ages from the published literature. (B) Maps showing the location of the study area within the context of the region east of the NPI and southern South America, including Lago General Carrera/Buenos Aires (GCBA) and Lago Cochrane/Pueyrredón (CP).

Table 1
Landform identification criteria used in this study, after Glasser et al. (2005, 2008), Bendle et al. (2017b), Darvill et al. (2017), and Chandler et al. (2018).

Landform	Morphology	ID criteria from imagery	ID criteria in field	Uncertainties	Significance
Ice-marginal glacial					
Moraine ridges	Linear, arcuate, curvilinear or saw-tooth shaped ridges of positive relief, orientated parallel, subparallel or perpendicular to the valley side. Ridges may project only part way across the valley from the valley side.	Smooth texture different from rough bare bedrock. Pale brown in colour where sparely vegetated. Lighter/darker shading on opposite flanks indicates ridge crest.	Prominent feature of positive relief. Morphology as described. Often found in association with glacially-transported boulders.	Unidentifiable from satellite images in well vegetated areas. Ridges of low relief may be difficult to detect. Possible confusion with trimlines.	Mark position of former ice margin. Can be dated to provide temporal context.
Ice-contact slope	Gently-sloping surface, from valley floor up to morainic deposit (e.g. terminal-moraine ridge). Slope commonly orientated along valley.	Uniform surface texture and colour. May show steep break in slope at top, or grade smoothly onto morainic deposit surface.	Visible as extensive area of sloping, uniform terrain.	May be difficult to identify on a low-resolution DEM if change in elevation across slope is small.	Marks terminal position of ice margin.
Morainal bank	Wedge shaped positive topography over a km scale with one very gently-sloping ice-proximal side and one more steeply-sloping ice-distal side, separated by a crest marked by horse-shoe shaped crescentic scars.	Extensive area of well-vegetated, uniform texture. May show sinuous, linked palaeochannels.	Visible as extensive area of very gently-sloping, uniform vegetated terrain.	May not be obvious in field if well-vegetated and due to the very gently-sloping surface.	Marks terminal position of ice margin. May indicate subaqueous deposition and lacustrine glacier termination.
Kettle hole	Rounded depression within area of morainic or glaciofluvial material (e.g. kame terrace).	Often filled with water but can also be dried. May be vegetated. Contrast in colour from surrounding terrain. Rounded form, associated with morainic complexes or glaciofluvial deposits.	Rounded depression visible from a position of higher topography. May be able to walk into depression if not filled with water.	More obvious from satellite imagery. Can be confused with small lakes formed in bedrock or non-ice related depressions.	Indicates previously-glaciated area and area of deposition of morainic or glaciofluvial material.
Subglacial					
Ice-scoured bedrock	Areas of bare or sparsely-vegetated bedrock with visible inherent structures.	Dark brown to grey to pink. Rough and irregular surface texture with visible joints, faults and fractures, distinctive from neighbouring sediment cover.	Rough texture and inherent structures evident. Distinctive in colour. Spatially extensive. Not practical to map in detail in the field.	May be difficult to distinguish from areas of thin/sparse sediment cover over bedrock, where boundary is gradational.	Shows areas of extensive ice at its pressure melting point.
Glacial diamicton	Gently-mounded material deposited on bedrock, ranging in extent, often on valley sides.	Yellow/pale brown in colour, with smooth texture in contrast to often neighbouring rough bedrock. Can be found in association with small channel gorges with clear breaks in slope. Often vegetated.	Where accessible and exposed (e.g. road cuttings) material can be identified as diamicton. Often difficult to identify due to inaccessibility and/or vegetation cover.	May be difficult to distinguish where cover is thin and boundary with bedrock is unclear	Indicates area of glacier deposition.
Flutes	Linear, elongated, parallel features formed in sediment	Occur in groups, often aligned differently to any inherent bedrock structure. May appear dark and light on opposite sides indicating positive relief. Commonly found in high-mountain areas in this study region, close to glacier cirques, and recently exposed (inside Little Ice Age moraines).	May be visible from distance although best identified from satellite imagery as spatially-extensive and can be partly obscured locally by vegetation or hidden in high-mountain areas.	Potential confusion with bedrock structures or medial moraines. Difficult to identify if short in length.	Indicative of former flow direction of warm-based ice and fast ice flow when laterally-extensive and highly-attenuated.
Glaciolacustrine					
Raised deltas	Flat-topped, steep-sided surface extending along and out from valley side, above valley floor, at the opening of a ravine. Often found in stepped sequence, incised by a palaeo or active river channel.	Uniform smooth-textured surface, in contrast to often adjoining rough bedrock. Light/dark contrast indicates breaks of slope at former delta front and incised channel.	Levels above the valley floor, in stepped sequence with an incised channel is often clearly visible from distance/opposite side of valley.	May be misidentified as a shoreline or kame terrace due to its planar nature at the valley side.	Height at the delta front at break of slope indicates former lake level.
Ice contact fan	Surfaces sloping to the valley floor from a flat/more gently-sloping top surface, the two separated by a slight break in slope.	Uniform smooth-texture surface may be vegetated. Contains sinuous lines of light/dark contrast indicating palaeochannels, which may also be wider and densely-vegetated with light/dark breaks in slope at their edge.	Prominent feature of positive, sloping relief above the valley floor. Large channels cut into the feature may be visible in the field.	May be misidentified as a raised delta due to its similar sloping morphology, although distinctively lacks a clear valley sediment source (ravine).	Indicates the frontal ice position of a marine or lacustrine-terminating glacier.

Palaeoshorelines	Narrow terrace surface on valley side with break in slope away from the valley side.	Approximate constant-elevation surface locally along valley. Light/dark contrast either side of break in slope. May be contrast in vegetation cover. Distinctive from exposed bedrock.	Often visible in the field as a distinctive flat surface on the valley side elevated above the valley floor. Especially identifiable when laterally-extensive.	May be misidentified as a kame terrace, although such a feature would be expected to gently slope down valley. Difficult to identify if discontinuous and/or well-vegetated	Indicates the former lake level.
Glaciofluvial					
Outwash plain	Large, gently-sloping flat plain cut by palaeochannels. Grades from former ice limit (e.g. a moraine ridge).	Large, smooth surface, uniform in texture and colour, and in contrast to surrounding topography. Palaeochannels on surface identifiable by light/dark colour change indicating negative relief. Also highlighted by vegetation change.	Extensive, flat, gently-sloping plains are visible in the field. Palaeochannel depressions can also be visible when looking across the plain's surface.	Exact limits of outwash plain may be difficult to distinguish.	Indicates major meltwater outflow pathways.
Fluvial terraces	Terraces running extensively along the valley side, extending out into the valley, sloping gently down valley and often stepped, separated by breaks in slope.	Uniformly-textured, vegetated surface. Break in slope is often unvegetated and lighter in colour. Often occur next to an active river system.	Visible in the field as terraces running extensively along the valley side above the valley floor, with steep scarp slopes visible along their edge.	May be mistaken for kame terraces or shorelines, although are distinctively stepped and may be more laterally extensive away from the valley side.	Indicate the former floodplain of a river and subsequent down cutting. May be indicative of a drop in base level and/or decrease in sediment supply.
Palaeochannels	Linear channels forming shallow depressions or deeper incisions. May have gently or steeply-sloping slides with scarps. Incised into fluvial, glaciofluvial, or glacial deposits.	Often appear darker than surrounding sediment and preferentially vegetated. May be sinuous, braided and extensive over valley-fill flood and outwash plains.	Visible in field as deep gorges or shallow laterally-extensive channels.	May be mistaken for breaks of slope at edge of outwash plain. Shallow palaeochannels often not visible in satellite imagery and certainly not on widely-available low-resolution DEMs.	Indicative of former path of river/stream flow. Deep incision may indicate drop of base level.
Kame terrace	Flat-topped surface above valley floor, gently-sloping down valley, extending from valley side. Pitted surface with steep ice-contact face.	Uniform surface texture and colour. Sharp break at ice-contact edge and surrounding terrain shown by shadowing/change in colour and texture. May be well-vegetated. Often associated with moraine ridges extending cross valley from terrace at valley side. No clear valley-side sediment source or catchment	Visible in field as large flat-topped feature, steep-sided, extending down valley, abruptly placed against steep valley-side bedrock in places.	May be confused with shorelines or raised deltas. Raised deltas have clear valley-side sediment source. Shorelines may be found more extensively, spanning multiple valleys. May not have a pitted surface.	Marks position of former lateral or frontal ice-margin and indicates ice thickness. Suggestive of high meltwater discharge and sediment transport.
Boulder bar	Elongated, positive relief, valley-floor feature with tapered ends. 100 s m in length.	Uniformly-textured, apparently-flat surface appears speckled with vegetation.	Visible in the field as an isolated, large feature in the valley floor. Boulders present on the surface.	Possible confusion with a point bar.	Often indicative of a large-hydrological-erosion and sediment-transport event, such as a flood. May form as a result of a glacier lake outburst flood in a glaciated region.
Paraglacial					
Alluvial fans	Sloping fans from valley sides fed by a small river or stream.	Smooth surface, splaying out in fan shape from valley side on to valley floor. Sharp boundary with surrounding topography through change in vegetation cover.	Distinct morphology identifiable from enough distance to provide context within valley. Cobble/gravel texture may be identifiable from distance.	Possible to misidentify as palaeo-delta or ice-contact deposit although unlikely.	Reworking of unconsolidated material by meltwater channels and streams.
Debris slopes	Steeply-sloping surface of sediment at the valley side, accumulating and sloping gently at valley floor. Can be laterally-extensive or more locally-confined.	Grey/pale brown in colour depending on composition. Smooth texture, may contain series of cone forms. Largely unvegetated. Common in high-mountain settings above upper vegetation line but also found as shattered bedrock and remobilised moraines in low valleys.	May be visible from valley floor. Texture, colour, morphology and composition clear when visible and/or accessible. Likely to be inaccessible and not visible in high-mountain settings.	Limits of extent in high-mountain areas above upper vegetation line may be difficult to identify.	Indicates paraglacial processes.
Floodplain	Sediment accumulated in valley floor often cut by a braided river system and found in association with channel bars.	Flat surface in valley floor cut by river system. Densely vegetated in places, often between braided active or palaeochannels.	Visible from valley side and on surface if accessible.	Possible confusion with outwash plain although more densely-vegetated and clearly associated with an established fluvial system.	When abandoned, may indicate area of past paraglacial activity. May contain active glaciofluvial system.

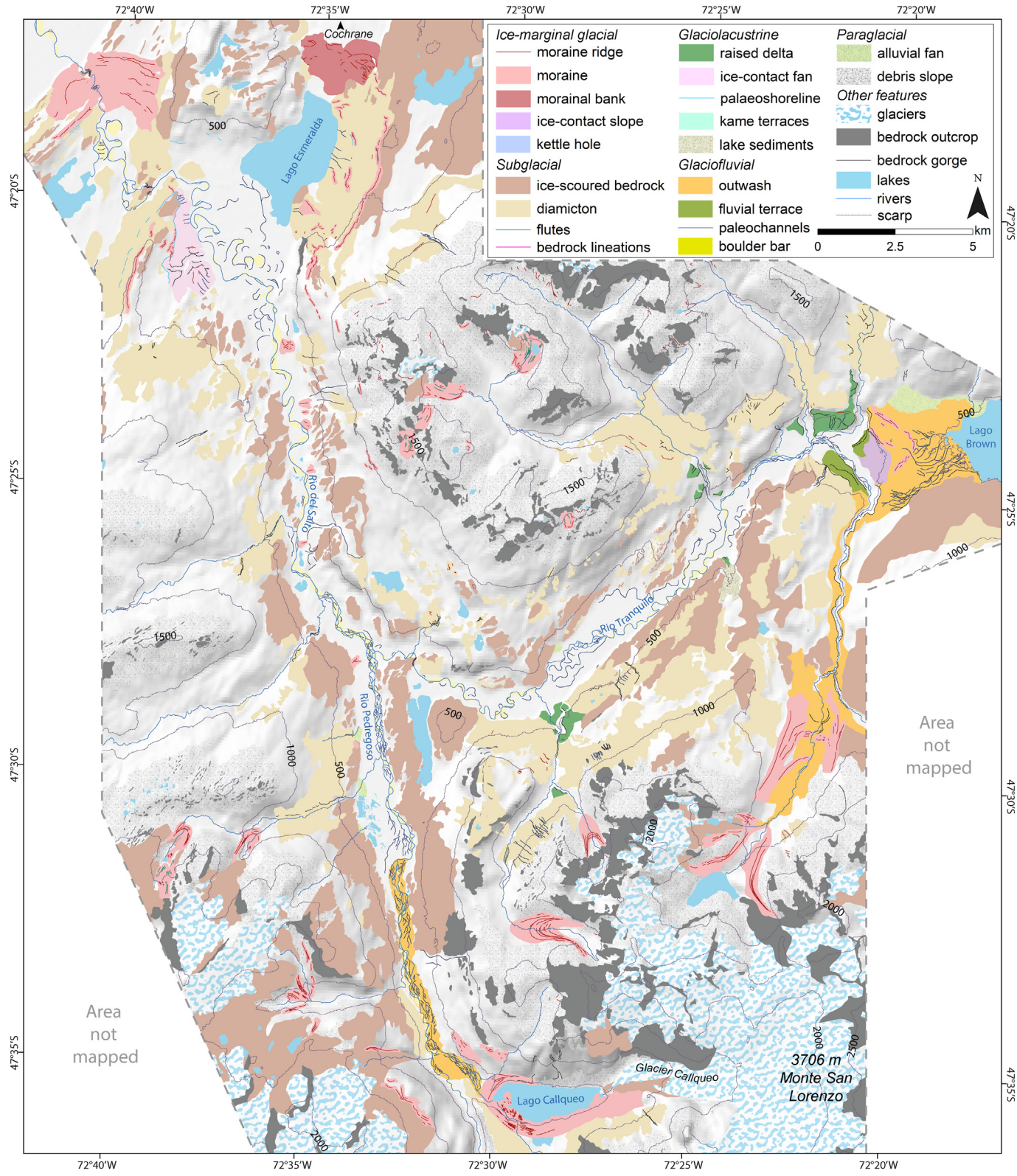

Fig. 2. Geomorphological map of the study region to the north of Monte San Lorenzo, including the Pedregoso, Salto and Río Tranquilo valleys. 500 m interval contour produced from ASTER DEM. A high resolution version of this map is available in the Supplementary Information.

gorges. Mapping of sections of the Upper Tranquilo valley and eastern Tranquilo valley is in part after Araya et al. (2014). Mapping in the north of the Salto valley is after Davies et al. (2018).

Critically, using field mapping to assist mapping from satellite imagery, we have identified 14 primary moraine sets (labelled M1a, M1b and M2 to M13) including 7 newly identified ice margin positions (M5 to 8 and M10 to 12) (Fig. 3). Previously identified sets have been ground-truthed and extended in their mapped extent. The Esmeralda and Brown moraines are labelled M1a and M1b respectively, as the furthest advanced moraine sets in their respective Salto and Tranquilo valleys. Moraines of the same colour are interpreted as forming coevally as part of the same moraine system.

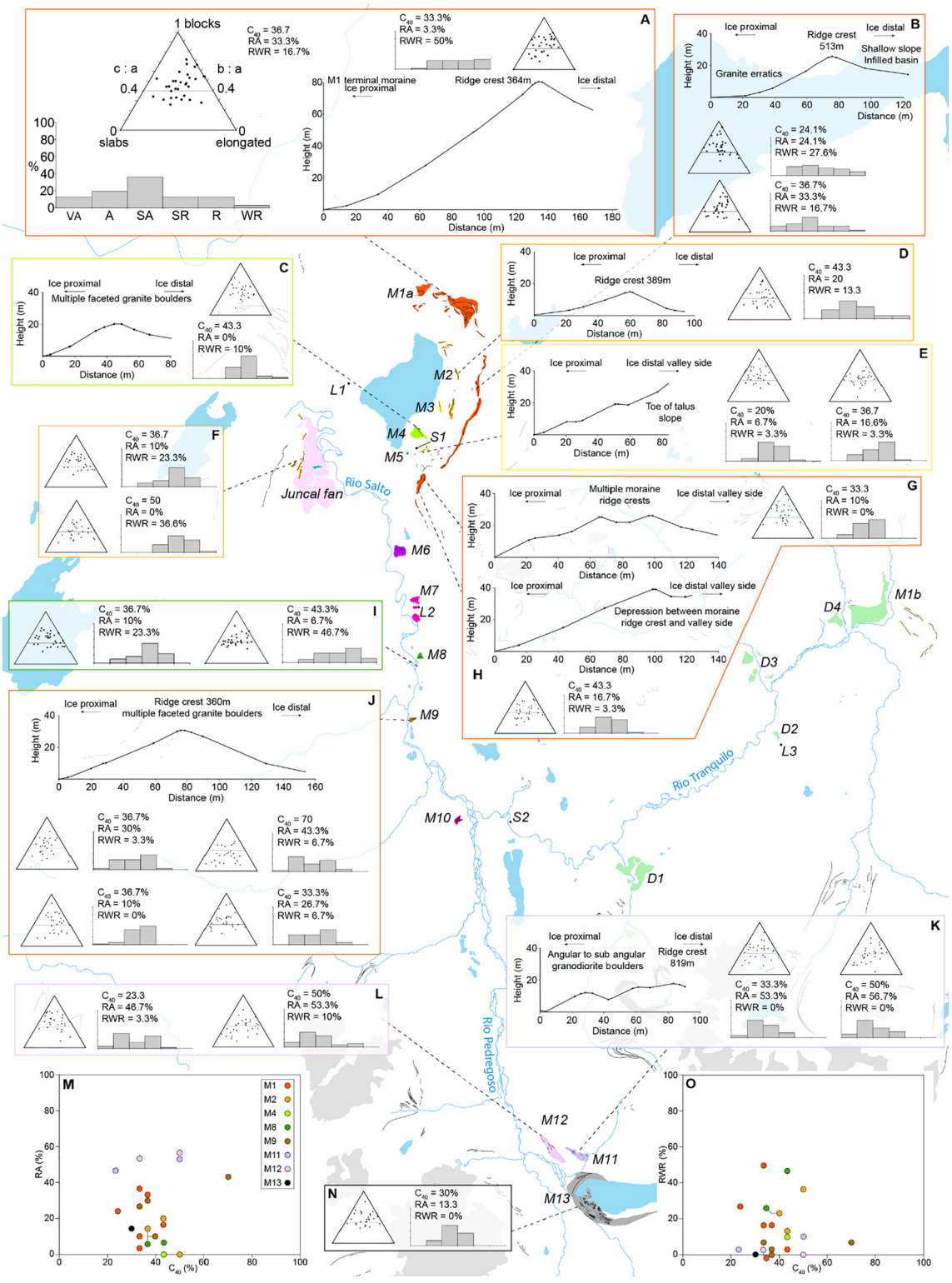

Fig. 3. (A) to (N) Moraine profiles and clast-shape data from sites along the Salto and Pedregoso valleys. (M) and (O) show RA-C_{40}% and RWR-C_{40}% plots respectively. Moraine sets, delta, lake sediment and diamicton section sites are labelled M1 to M13, D1 to D4, L1 to L3 and S1 to S2 respectively.

4.2. Ice-marginal sediment-landform associations

4.2.1. Frontal moraines

The Esmeralda (M1a, cf. Davies et al., 2018) and Brown (M1b) moraines situated at the northern and eastern ends of the Salto and Río Tranquilo valleys respectively are the most substantial frontal moraines. The M1a frontal moraine has been dated to the ACR and formed coevally with the 7.5 km long, valley-parallel lateral moraine component (Davies et al., 2018) (Fig. 3). We speculate that the M1b moraine also formed at this time, due to their similar relative size and position in the Tranquilo valley (Fig. 3). Inset of M1a in the Salto valley are a series of cross-valley, sharp-crested, both arcuate and more straight frontal moraines (M4 to M9) formed sequentially after the ACR, positioned periodically along the eastern valley side stretching south until

the confluence with the Río Tranquilo valley. They are up to 40 m in height above the valley floor and up to 300 m long (Fig. 3). M4 (also known as the "Moraine Mounds", ca. 12.3 ± 0.4 ka cf. Glasser et al., 2012; Davies et al., 2018) and M6 are associated with semi-isolated masses of moraine producing an uneven surface of material on the ridges' ice-proximal side (Figs. 2 and 3). M6, 7, 8, and 9 notably extend perpendicular from terraces on the eastern valley side, only part way across the valley floor, east of the Río Salto (Figs. 2 and 3). The moraine ridges are composed of stratified massive and laminated sands, coarse sub-rounded to sub-angular gravels, and diamictons (e.g., M5: Figs. 3E and 5, M8: Figs. 3I and 6). Multiple sub-rounded to sub-angular, faceted granitic to dioritic boulders, up to 1 m in size, can be found along the ridge crests, strewn over larger areas of associated morainic material and within exposed sections.

Across the study area, clast-shape data taken from moraine sites shows predominantly blocky clasts, with C_{40} percentages below 50% (Fig. 3). The moraines in the Salto valley are dominated by sub-angular to sub-rounded clasts, whilst those in the Tranquilo valley have a largely sub-angular to very-angular form. The M1b moraines consist of a series of discontinuous, sinuous ridges between 60 and 700 m long, arranged in an arcuate form, spanning 2 km across the valley. They occur on a topographic high, ca. 120 m about the valley floor to the east, with a steep ice-contact slope on the western, ice-proximal side, and a more gently-sloping outwash plain on the eastern, ice-distal side.

4.2.2. Lateral moraines

Valley-parallel, lateral moraine ridges in the study region have three primary morphologies. The first are large, laterally-extensive ridges with narrow crests and broadly symmetrical sides (Fig. 3M1 to M3, Fig. 7A, C to F). The second group consists of smaller, closely-spaced pairs or groups of laterally-discontinuous ridges with broadly equally-dipping sides, dissected by meltwater channels. They are found on topographically-flat bedrock plateaus on the northern flank of Cordon Esmeralda below M1 and at the southern end of the Salto valley (M11 and M12) (Fig. 3). The third are small, discontinuous, ridges up to a meter high and 100 m long, found on the sloping valley side southeast of Lago Esmeralda, between M1 and M4, forming the lateral component of M3 (Fig. 3).

The ACR M1a (Davies et al., 2018), M1b and post ACR M2 ridges are characterised by massive, silty and sandy diamictons and gravels, with numerous faceted granitic and dioritic cobbles and boulders up to 2 m along the a-axis (Figs. 7A, 8). M2 is overtopped by poorly defined units of clast-supported, sandy coarse gravel, and clast-supported silty fine gravel, edge rounded and faceted pebbles. Stones are primarily sub-angular to sub-rounded, blocky and elongated (Fig. 3D).

4.2.3. High-altitude valley moraines

Alongside the moraines in the lower valleys, well-preserved late Holocene lateral and frontal moraines are found close to the present-day Calluqueo glacier margin (Fig. 2), in part damming Calluqueo proglacial lake, and in high altitude cirques in the upper Tranquilo valley and on Cordon Esmeralda. The largest Calluqueo moraine (M13) manifests as a sharp-crested, steep-sided arcuate frontal terminal moraine ridge, ca. 100 m above the valley floor and a broader-crested lateral moraine on the southern side of Lago Calluqueo. Numerous smaller, closely-spaced sinuous elongated parallel ridges are found along the broad lateral moraine ridge at the southwestern end of the lake. They are up to 3 m high with surfaces scattered with numerous lose, angular to subangular granodiorite cobbles and boulders. The small valleys on Cordon Esmeralda also contain numerous well-preserved, densely-spaced terminal ridges close to cirques, between 5 and 20 m apart superimposed over valley-parallel flutings (Fig. 10). In front of these are larger moraine ridges with a classic saw-tooth morphology (cf. Evans et al., 2017).

4.2.4. Meltwater channels

Meltwater channels are found in association with the groups of laterally-discontinuous ridges on the bedrock plateaus on the northern flank of Cordon Esmeralda below M1. The largest is a gently-sloping, approximately-straight channel running the 200 m along the length of the complex, parallel to contemporary contours and the axis of moraine ridges. We interpret this channel as ice-marginal (Greenwood, 2007). There is a notable lack of meltwater channels observed elsewhere.

4.3. Subglacial associations

4.3.1. Ice-scoured bedrock

Isolated areas of ice-scoured bedrock occur along the lower sides of the Esmeralda, Salto and Río Tranquilo valleys, obscured in places by vegetation cover and separated by areas of diamicton plastered on to the valley sides and floor (Fig. 2). It is not found at higher elevations or topographic crests between valleys, where instead bedrock crops out as blocky or sharp-sided exposures. Ice-scoured bedrock is also reported in neighbouring valleys east of the NPI (Glasser et al., 2009; Bendle et al., 2017b; Davies et al., 2018). Bedrock lineations can be identified orientated broadly NE-SW at the confluence of the Salto and Río Tranquilo valleys on a bedrock high set away from the valley side (Fig. 11).

4.3.2. Glacial diamicton

Areas of diamicton can be found plastered along the valley sides and at elevations both above and below ice-scoured bedrock. A flat-topped surface of diamicton is found on the eastern side of the Esmeralda valley on the western flank of Cordon Esmeralda (Figs. 3S1, 9) showing a stone-rich, silty diamicton, stratified into a clast-supported layer below a matrix supported layer. Both layers contain boulders up to 30 cm in size. A small section of laminated sands is found at the base of the lower unit. Near the confluence of the Esmeralda and Río Tranquilo valleys (Fig. 3S2), a road cutting reveals a section of sediment plastered onto the side of bedrock. This comprises a silty diamicton, stratified in places, containing faceted boulders and rich in striated, faceted stones and interbedded with a layer of stratified, planer-bedded gravels. These are disrupted by inverted triangular structures of massive gravels. The lower diamicton is dissected by a sub-vertical unit of matrix-supported massive gravel and contains a discontinuous unit of partly-laminated medium sand at its base.

4.3.3. Flutes

In the high-altitude cirque on Cordon Esmeralda elongated parallel flutings 3 m to 7 m wide run along the valley length, found in association with closely-spaced moraine ridges, inset of large saw-tooth moraines (Fig. 10). They are predominantly straight but curve with the profile of the valley. They are not found in the less recently deglaciated lowland Salto, Pedregoso and Tranquilo valleys.

4.4. Glaciolacustrine associations

4.4.1. Raised deltas

Large flat-topped, steep-fronted bodies of sediment are found along the length of the Río Tranquilo valley at three main sites: the western end (D1), centre (D2 and D3) and eastern end (D4) of the valley (Figs. 2 and 3). They are found in stepped sequence, incised by active and abandoned river channels at the opening of a ravine. Three primary terrace levels are defined: 600 m asl (at D1), 520 m asl (at D3 and D4) and 425 m asl (at D1, D2 and D3). D1 (Fig. 12) reveals alternating well-defined beds of clast and coarse sand matrix-supported gravels, coarse gravely sands and hyper-concentrated clast-supported cobble beds up to 50 cm in thickness. Clasts are sub-rounded to rounded. These beds dip at 25° west-northwest towards the valley floor and are overtopped and truncated by a coarse, clast-supported, cobble-rich gravel bed. At the northern end of the section, the dipping beds give way to a clast-supported unit of cobbles up to 30 cm in size (Fig. 12B). A section in the D4 delta (Fig. 4) reveals a structure of dipping foresets.

4.4.2. Morainal banks

Next to the steep-sided Esmeralda moraines (M1b) is a distinctly-different moraine landform interpreted as a subaqueous morainal bank formed at the ACR (Davies et al., 2018). It is wedge-shaped and dips gently west towards Lago Esmeralda while the eastern flank is much steeper. Exposures show a silty, stone-rich diamictic composition interbedded with sands and gravels (Davies et al., 2018).

4.4.3. Glaciolacustrine sediment

Roadside exposures north of Lago Esmeralda show diamicton overtopped by 2 mm thick silt and clay rhythmites with isolated stones (Figs. 3L1, 13A). Similar facies are found on the eastern side of the Salto valley within the broader M7 moraine complex (Figs. 3L2, 13B). A 3 m high section through the top of a small ridge reveals upward-fining sands overtopped with rhythmites, interbedded with sands at their

Fig. 4. Photo of cross-valley terminal moraines in the Esmeralda, Salto and Brown valleys. (A) Arcuate M4 moraine ridge in front of the Esmeralda 'Moraine Mounds'. (B) View south up the Salto valley and inset C. (C) M6 moraine and inset mounds. (D) Section through the M8 moraine ridge with associated kame terrace in the Salto valley. (E) M9 moraine ridge and associated kame terrace in the Salto valley. (F) Western end of the Brown valley, showing raised deltas and the inner M1b Brown moraine ridge.

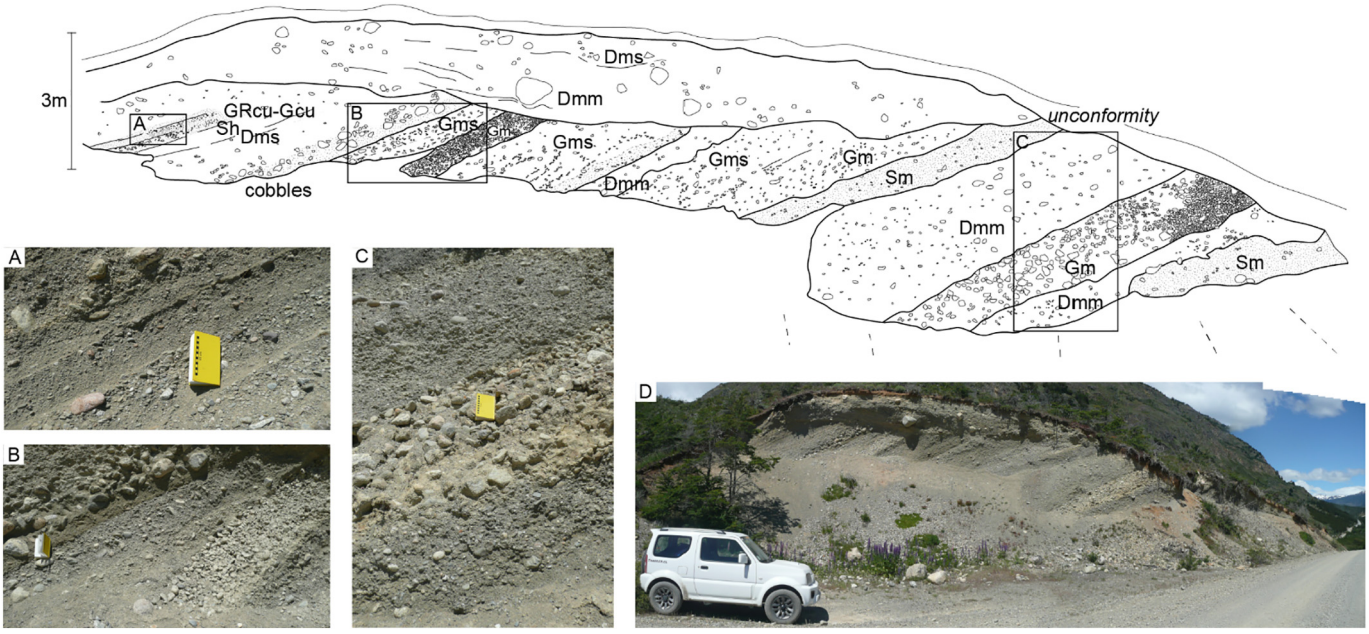

Fig. 5. Section and photos at the M5 moraine. (A) to (C) show zoomed in photos of section, their locations labelled on the sketch. (D) Photo of exposed section through the M5 moraine.

top, and a stone-rich silty diamicton. The rhythmites contain numerous dropstones with associated deformed and draped laminations. Up a small tributary valley from D2, between two bedrock highs are large roadside exposures of bedded sands and gravels (Fig. 3L3). On the western side is 4 m of well-sorted, bedded, fine sand with occasional gravel dropstones and ripple-cross laminations in places (Fig. 13C). This is

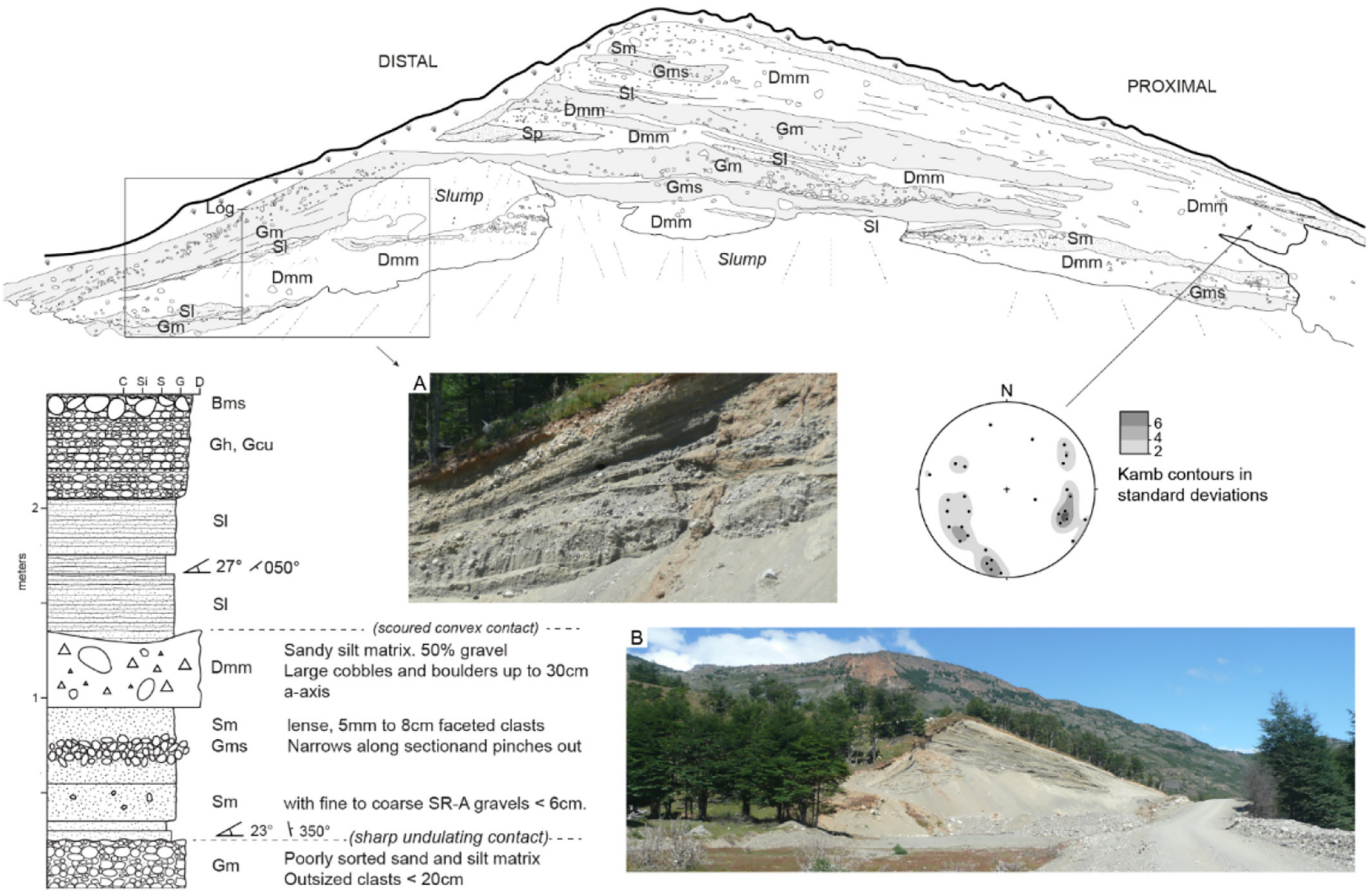

Fig. 6. Sedimentary section, log and stone data from a quarry section at M8. (A) Zoomed in photo of a section of the exposure on the ridge's distal side through which the sedimentary log was taken. (B) Exposed face in full.

Fig. 7. Photographs of lateral moraines in the Esmeralda and Salto valleys. (A) M2 lateral moraine, with context of Esmeralda terminal moraines (M1a) and Esmeralda 'Moraine Mounds' (M4). (B) Moraine ridge on the lower northern side of Cordon Esmeralda. (C) M2 lateral moraine ridge pair. (D) View north along the ridge crest of M1a lateral moraine. (E) View of a glacially-transported boulder on the ridge crest of M1a lateral moraine. (F) View of the M1a lateral moraine ridge on the north western flank or Cordon Esmeralda, looking down over the Esmeralda valley. (G) Boulder on a ridge crest within the M12 moraine complex. (H) Boulder strewn ridge crests in the M11 moraine complex.

separated by a sharp erosional contact from overlying trough cross-bedded, and then massive gravelly sands. These contain inclusions of planar laminated fine sands. On the eastern side of the tributary valley, and ca. 70 m below the western site, is a 6 m high exposure of well sorted sands with draped ripple cross-laminations and massive sand beds (Fig. 13D).

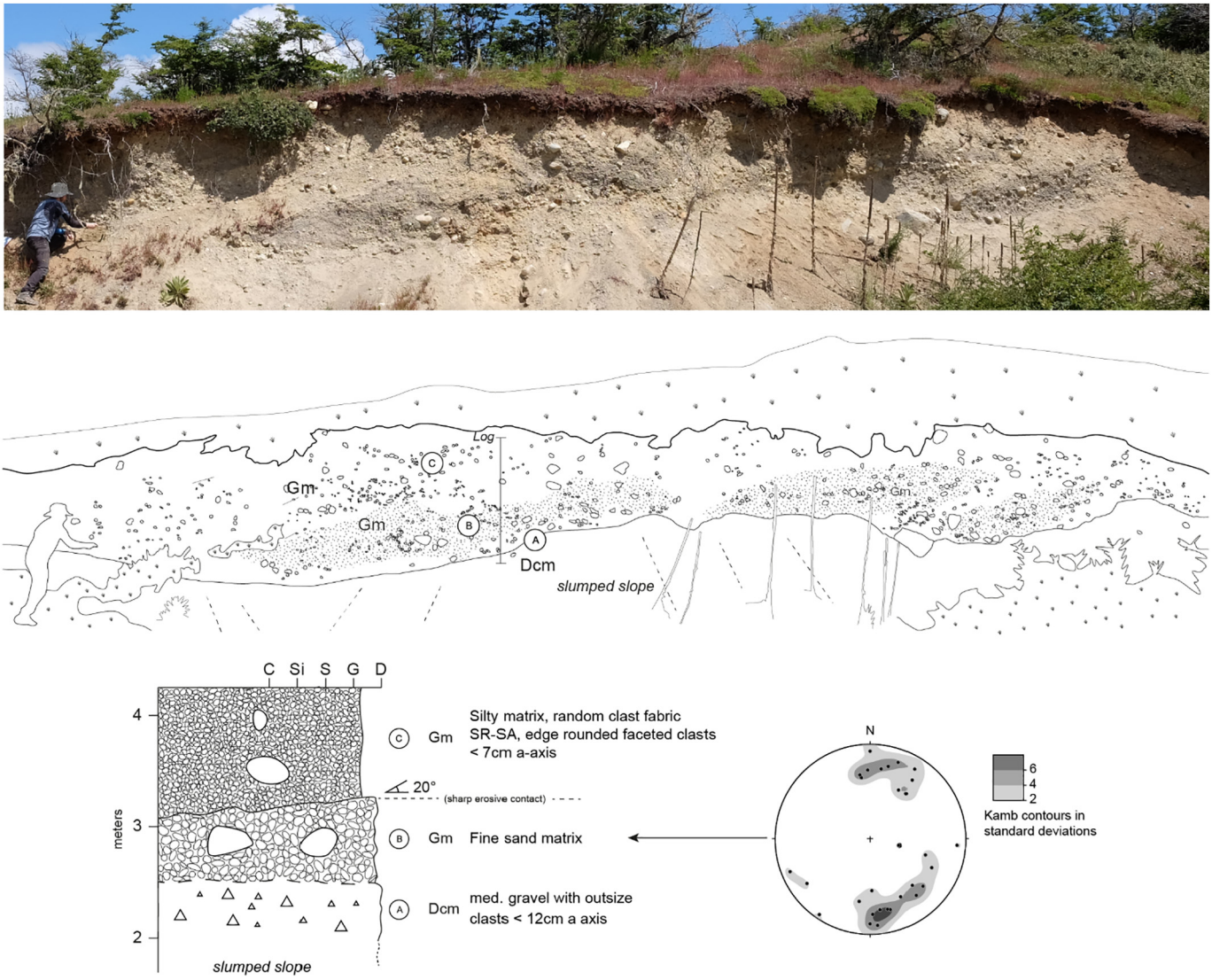

Fig. 8. Sedimentary log, section and clast fabric data of the M2 lateral moraine.

4.4.4. Palaeoshorelines

Inside the Esmeralda moraines, palaeoshorelines are carved into valley-side diamicton in the northern Salto valley on the eastern side of the Juncal Massif, on the southern side of Cerro Ataud and southeast of Lago Esmeralda (Davies et al., 2018). The palaeoshorelines form of gently-dipping platforms with scarp slopes on the valley floor side, running flat or shallowly-dipping in long profile.

4.5. Glaciofluvial associations

4.5.1. Outwash plains

A palaeo-outwash plain of glaciofluvial sands and gravels is located east of the M1b moraines sloping gently down towards and terminating at Lago Brown (Fig. 2). The surface is covered by cross-cutting sinuous palaeochannels. Narrow valley constrained outwash, or 'valley trains', cover the entire floor of the southern section of the Pedregoso valley and contain active braided river channels.

4.5.2. Fluvial terraces

Stepped, fluvial terraces are found at the eastern end of the Tranquilo valley, either side of Rio Tranquilo (Fig. 2). The western terraces run for 1.6 km along the valley side on two levels, separated by a small scarp slope. The upper terrace slopes from 470 m to 415 m asl and the lower terraces slope from 450 m to 405 m asl, grading down to the valley floor level at their northern-most point. The two eastern terraces are adjacent to the ice-contact slope and grade south to the valley floor, with large scarp slopes on the northern sides.

4.5.3. Kame terraces

Along the eastern side of the Salto valley, masses of sediment with flat tops at ca. 370 m asl run discontinuously south to the confluence with the Río Tranquilo valley (Fig. 2). The top surface slopes gently away from the valley side before a steep break in slope forms a scarp down to the valley floor. The terrace surfaces are ca. 40 m above the valley floor, gently undulating and dissected by channels from the valley side. They contain hollows in places, some manifesting as lakes, producing kame and kettle topography (Livingstone et al., 2010). The largest terrace is 3.9 km long and up to 550 m wide, located just north of the confluence with the Tranquilo valley, and found in association with moraine ridge M9 (Fig. 4E). At the opening on the Salto valley, an exposure at the terrace base shows cross-bedded alternating coarse sands and gravels, dipping 20° southwest towards the valley floor, fining upwards in places (Fig. 14). Pebbles are faceted and edge-rounded and can be

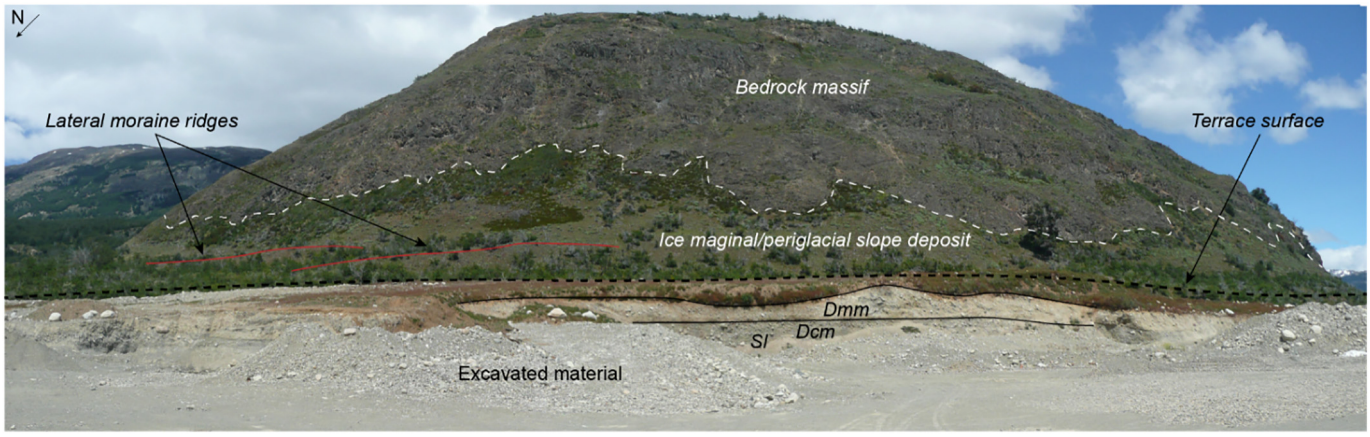

Fig. 9. Section through diamicton at site S1 to the southeast of Lago Esmeralda, with lateral moraine ridges in Fig. 7B visible on the side of the slope.

found in lags at the base of beds. These alternating sand and gravel beds are topped by gravel lenses and broad, shallow scours of trough cross-bedded gravels and sands.

4.5.4. Boulder bar

Inset of the terminal Salto moraine complex is an elongated, 360 m long by 160 m wide bar of morainic material (Figs. 2, 15C), topped by sporadic boulders on its surface. Its elongated, tapered form is analogous to boulder bars observed in valleys to the north, formed by large outburst floods of Lago General Carrera/Buenos Aires likely reworking valley floor morainic material (Thorndycraft et al., 2019).

4.5.5. Fluvial bars and palaeochannels

Both mid-channel, bank-attached and point bars are found as part of the active Rio Tranquilo, Pedregoso and Salto glaciofluvial systems (cf. Collinson, 1996). Palaeobars are found on the floodplain bordering these rivers and in conjunction with glaciofluvial palaeochannels (Fig. 15).

4.6. Paraglacial associations

4.6.1. Floodplain

The floors of the Salto and Tranquilo valleys are covered by floodplain associated with sand and gravel bar deposits. This differs from the morphology of the outwash plain east of the M1b Brown moraines, which is built up above the level of the valley floor. Numerous abandoned river-channels are found across the valley floor throughout the Salto and Tranquilo valleys and within the floodplain are a number of small lakes infilling pits (Fig. 15) (cf. Benn and Evans, 2010; Brynjólfsson, 2015; Giles et al., 2017).

4.6.2. Slope deposits

Unvegetated, modified drift-mantled slopes are found at the sides of the most recently deglaciated (post-LIA) valleys. They comprise upper sections of gullies cut into glaciogenic deposits (including lateral-moraine ridges), above coalescing debris cones and fans of reworked sediment (cf. Curry, 1999; Ballantyne, 2002; Curry et al., 2006). The clearest example is on the northern and southern valley sides above Lago Calluqueo. We also find examples of paraglacial rock-slope failure.

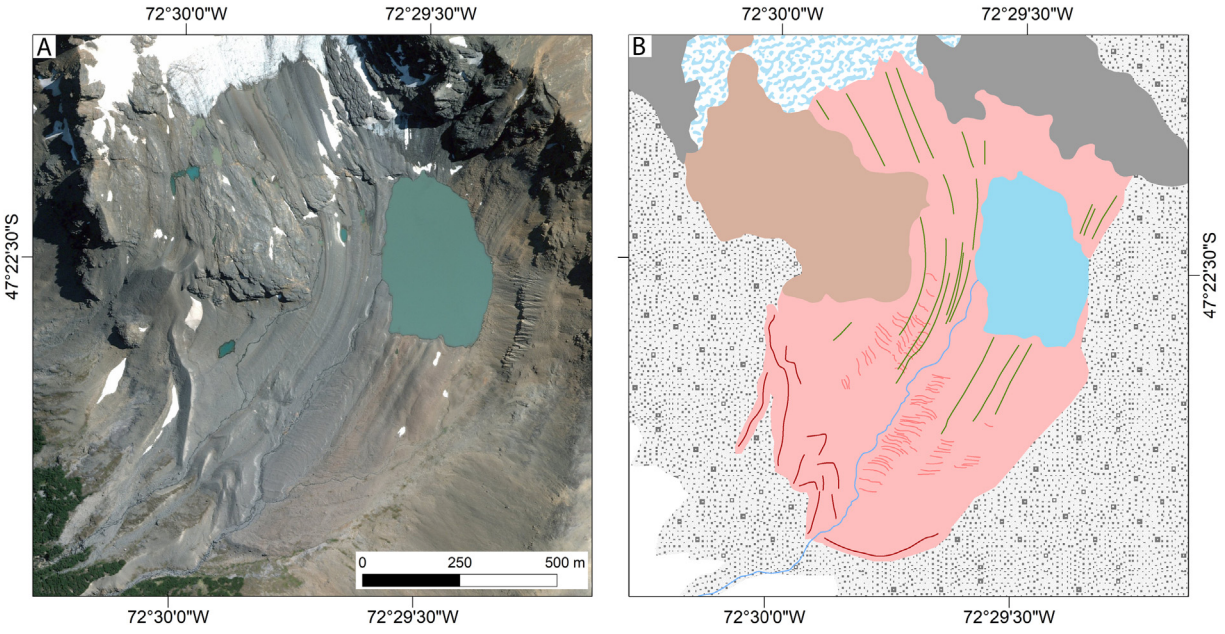

Fig. 10. (A) Satellite image (Digital Globe Esri™) of cirque on Cordon Esmeralda. (B) Mapped landforms from satellite image in (A). Colours correspond to key in Fig. 2.

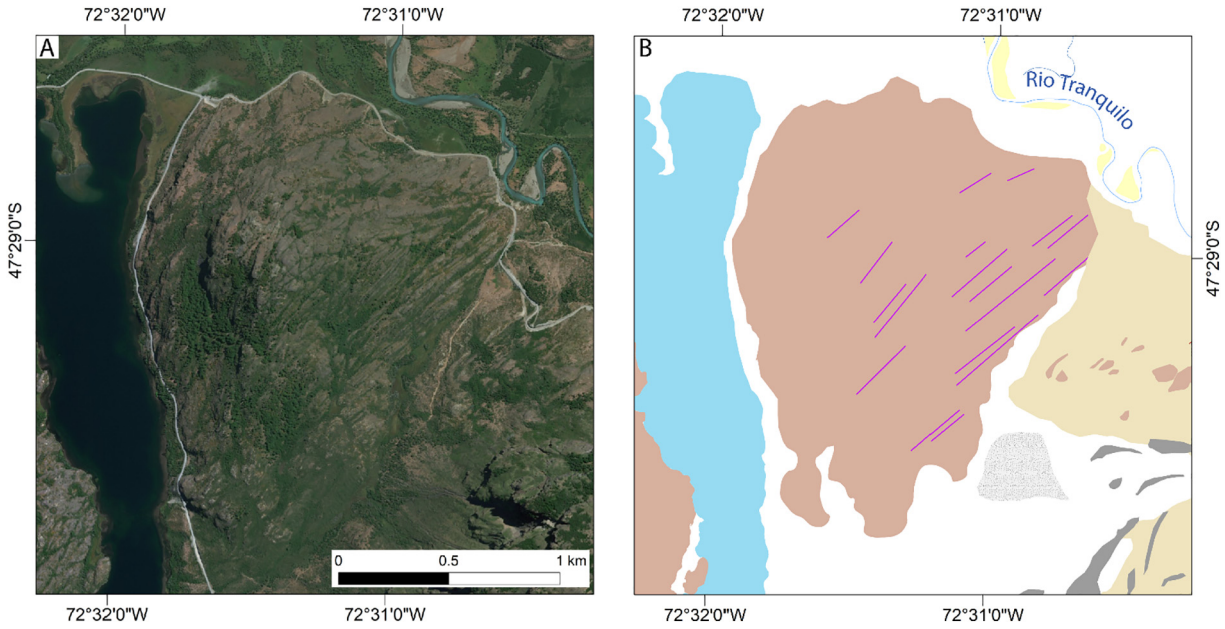

Fig. 11. (A) Satellite image (Digital Globe Esri™) of the confluence of the Salto and Río Tranquilo valleys. (B) Mapped landforms in area (A) showing ice-scoured bedrock and lineations. Colours of landforms reflect those in Fig. 2.

These are primarily talus accumulations high on the valley sides comprising angular boulders up to 15 m in size.

4.6.3. Alluvial fans

Alluvial fans are found at the opening of gullies at the sides of the Pedregoso and Tranquilo valleys, where the valley side meets the valley floor floodplain. They slope gently between 2° and 10°, are well vegetated, and often associated with active river systems and fluvial downcutting.

5. Discussion

The observed geomorphology and sedimentology of the Salto, Pedregoso, Tranquilo and surrounding high-altitude valleys allows us to produce landsystem models which operated during and following a period of late Quaternary warming. The region can be divided into distinctive areas whose core sediment-landforms associations are characterised by either glaciolacustrine, land-terminating glacial or mountain-valley landsystems. These are then overprinted by both glaciofluvial and paraglacial landsystems,

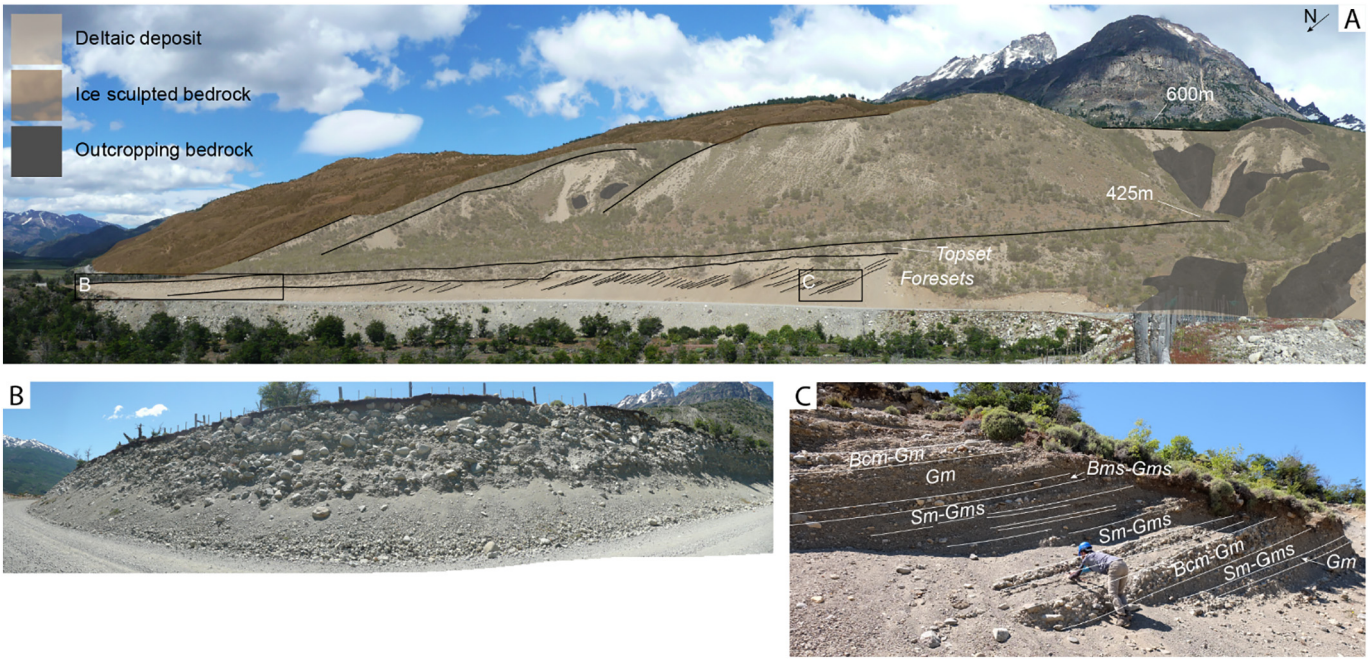

Fig. 12. (A) 600 m and 425 m stepped terrace on the southern side of the Tranquilo valley with an incised gorge on the right of the image. (B) The northern section of road cutting, composed of clast-supported cobbles. (C) The southern section showing dipping sand and gravel foresets.

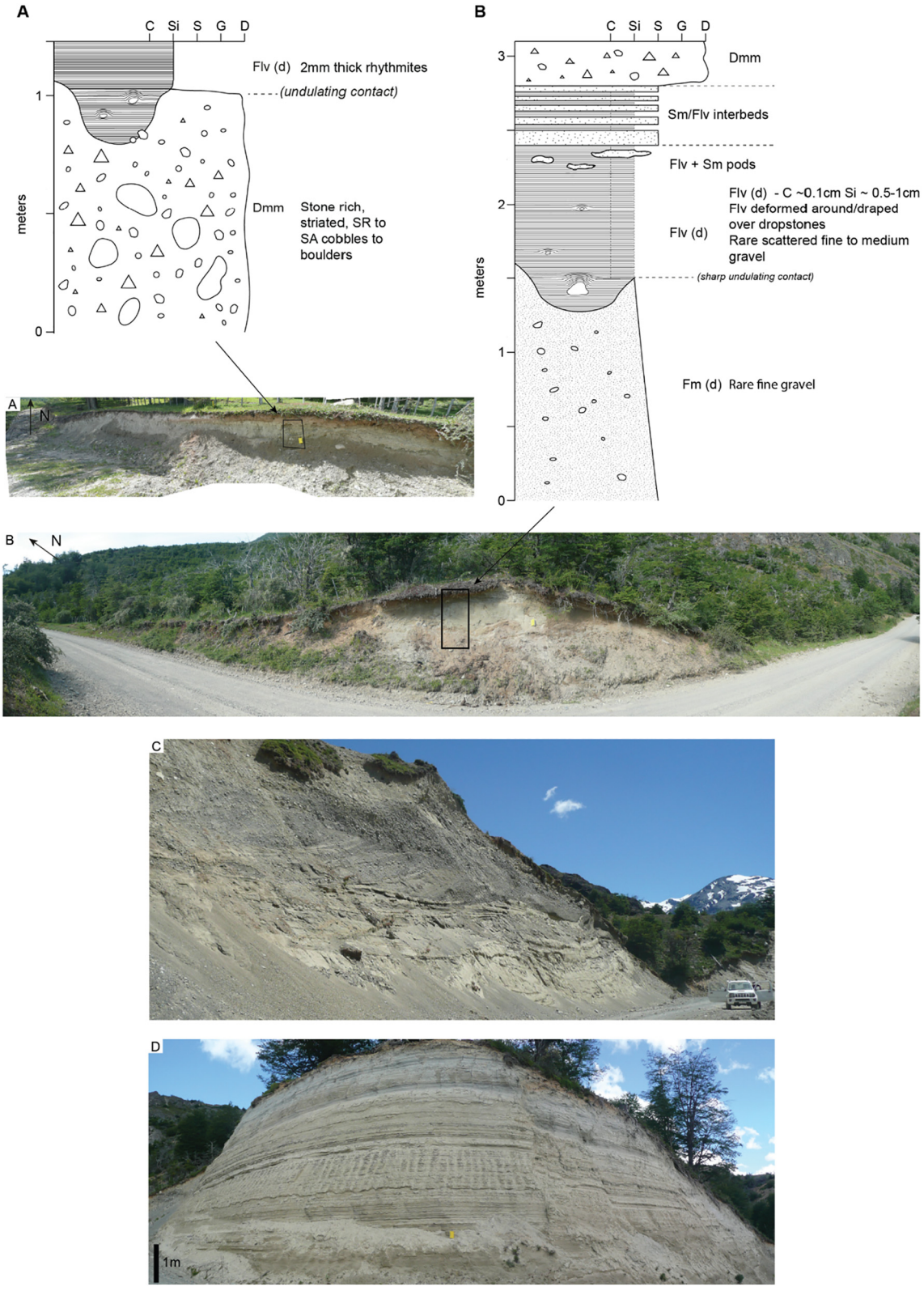

Fig. 13. (A) L1 section logged through roadside exposure north of Lago Esmeralda. (B) L2 section logged through roadside exposure in Salto valley through part of the M7 moraine complex. (C) L3 western section through roadside exposure of massive sands and gravelly sands. (D) L3 eastern section through roadside exposure through well sorted bedded sands.

with varying degrees of modification of the glaciated landscape. These palimpsest environments can be thought of as existing within an overarching glaciated valley landsystem acting as a 'family of landsystems', documenting significant variability (Benn et al., 2003).

5.1. Landsystems north of Monte San Lorenzo

5.1.1. Glaciolacustrine landsystem

The glaciolacustrine sediment-landform associations of the Tranquilo valley consist of raised stepped deltas and glaciolacustrine sand and

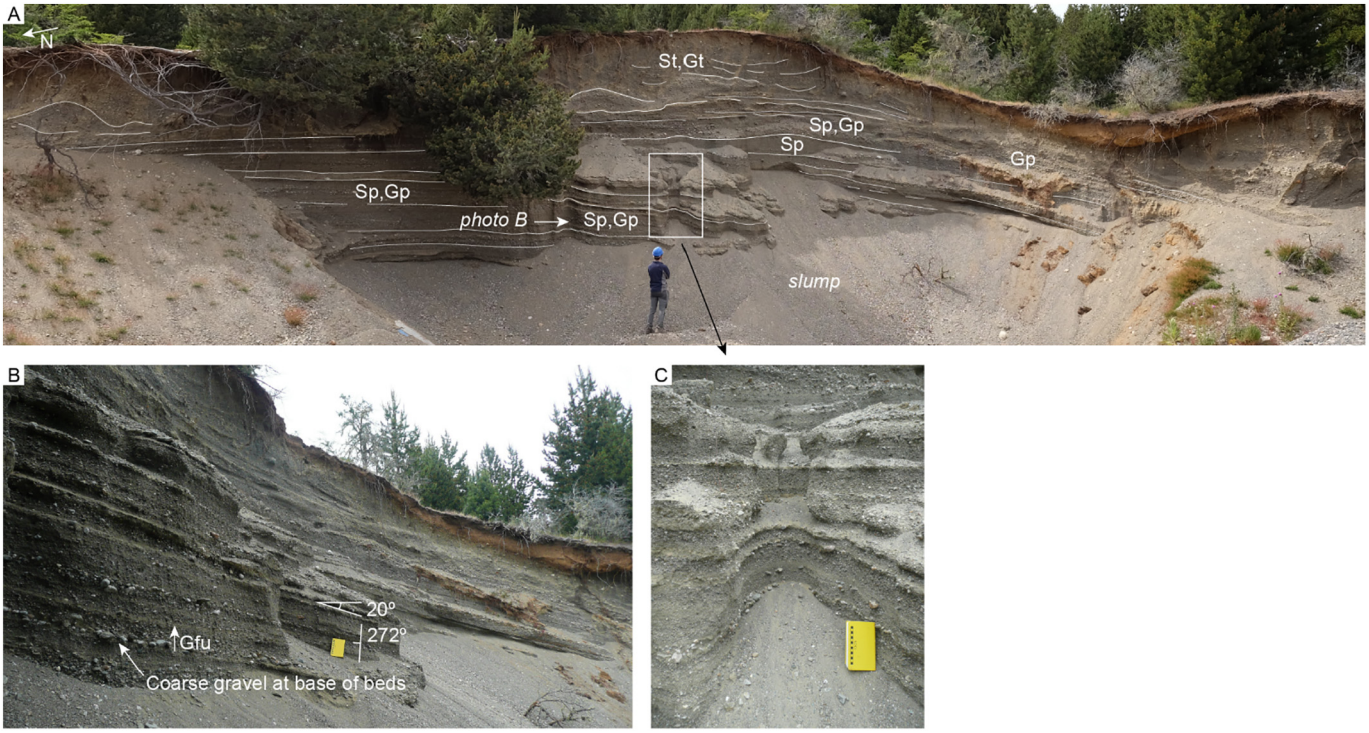

Fig. 14. Section exposing the sedimentary composition and structure at the base of a kame terrace on the eastern side of the opening of the Salto valley, south of Lago Esmeralda. (A) Overview of the section. (B) Photo taken looking left to right illustrating the dipping sand and gravel beds. (C) Close-up photo of dipping interbedded sands and gravels.

sandy gravel deposits. Deltas have the classic Gilbert form (Gilbert, 1885), deposited into a former ice-dammed lake (Ashley, 2002; Longhitano, 2008; Benn and Evans, 2010), and are analogous to those found around the margins of Lago General Carrera/Buenos Aires (Bell, 2008, 2009; Glasser et al., 2009; Bendle et al., 2017b) and in the Torres del Paine region of Patagonia (García et al., 2014), as well as in the Thompson valley in British Columbia (Johnsen and Brennand, 2004, 2006) and at Glen Roy (Peacock, 1986; Palmer and Lowe, 2017; Sissons, 2017), the northern Cairngorms (Brazier et al., 1998) and Achnasheen, Scotland (Benn, 1989, 1992). Alongside the glaciolacustrine sediments, they provide evidence for the palaeolake Tranquilo occupying the Tranquilo valley at 520 m asl and then 425 m asl following punctuated lake drainage (Fig. 16).

The D1 delta terrace (Figs. 3, 12A) at 600 m asl likely reflects a higher elevation ice-marginal lake formed when ice occupied the Tranquilo valley, damming valley side tributaries. Further, such higher elevation terrace surfaces are found in neighbouring small tributary valleys. Deltas at D3 and D4 and bedded sands south of D2 indicate that when the lake level was at 520 m asl the frontal ice-margin sat between D2 and D3 and the confluence with the Salto valley for a period of relative stability or slow recession to allow for such masses of sediment to accumulate (Fig. 16C). The bedded sands at L3 likely formed through relatively low-energy deposition of well-sorted sediment into the lake. The draped ripple-cross laminations indicates a high rate of sediment aggradation relative to horizontal transport and flow (Evans and Benn, 2004). The formation of these deltas is reliant on both the presence of the large water body and local topography channelling rivers and fluvially-transported sediment from the mountain valley catchments through tributary valleys and gullies into the main valley. A topographic control is also evident through the absence of deltas in the northern Salto valley glaciolacustrine landsystem which lacks sediment input from tributary valleys.

The Brown moraines in the east sit on a topographic high with ridges up to ca. 535 m asl and a glacial outflow channel at ca. 520 m asl dissecting these ridges. An outwash plain east of the Brown moraines is incised by the large primary glacial outflow channel and multiple glaciofluvial braided palaeochannels. This provides evidence for a 520 m asl col. at the Brown moraines for the upper, 520 m asl palaeolake Tranquilo lake level and drainage to the east into Lago Brown and on into Lago Cochrane/Pueyrredón (Fig. 16B). With the Tranquilo valley floor dropping in elevation to the west, the lake was dammed by ice flowing north from the Pedregoso valley into the Tranquilo valley, having receded from its frontal position at the Brown moraines (Fig. 16B and C). Both topography and the location of the ice mass therefore control the extent and depth of the lake.

There is a notable absence of cross-valley ridges in the Tranquilo valley which could be due to a number of factors. Benn (1989) elucidates a requirement of grounding line stability for the formation of ridges at Achnasheen in Scotland. Subaerial cross-valley ridges formed in the neighbouring Salto valley during this same period suggest that periodic local ice stability did occur. Therefore the calving of ice into palaeolake Tranquilo may have caused the instability of the ice front and its steady continuous retreat (cf. Carrivick and Tweed, 2013).

Following ice recession a lower elevation drainage pathway, and potentially subglacial drainage indicated by a bedrock incised channel, opened into the Salto valley at the Tranquilo-Salto confluence and the lake stabilised at 425 m asl (Fig. 16D). This punctuated drainage and later final drainage of palaeolake Tranquilo may have resulted in outburst floods down the Salto valley. Evidence for large flood events may be provided by the aforementioned inset boulder bar of the Salto moraine complex, and bedrock incision in the lowermost reach of the Rio Tranquilo and in the middle of the Salto moraines, downstream of the Lago Esmeralda reach (Fig. 15C). The boulder bar and bedrock incision are consistent with flood evidence in the Baker valley (Thorndycraft et al., 2019).

Davies et al. (2018) present a glaciolacustrine landsystem model for the northern Salto valley to document the formation of the asymmetric Esmeralda moraine ridge and bank, and Juncal fan as part of a landform assemblage formed as ice terminated into Lago Chelenko palaeolake and subsequently receded to the more steeply topographically constrained section of the Salto valley south of the present-day Lago Esmeralda.

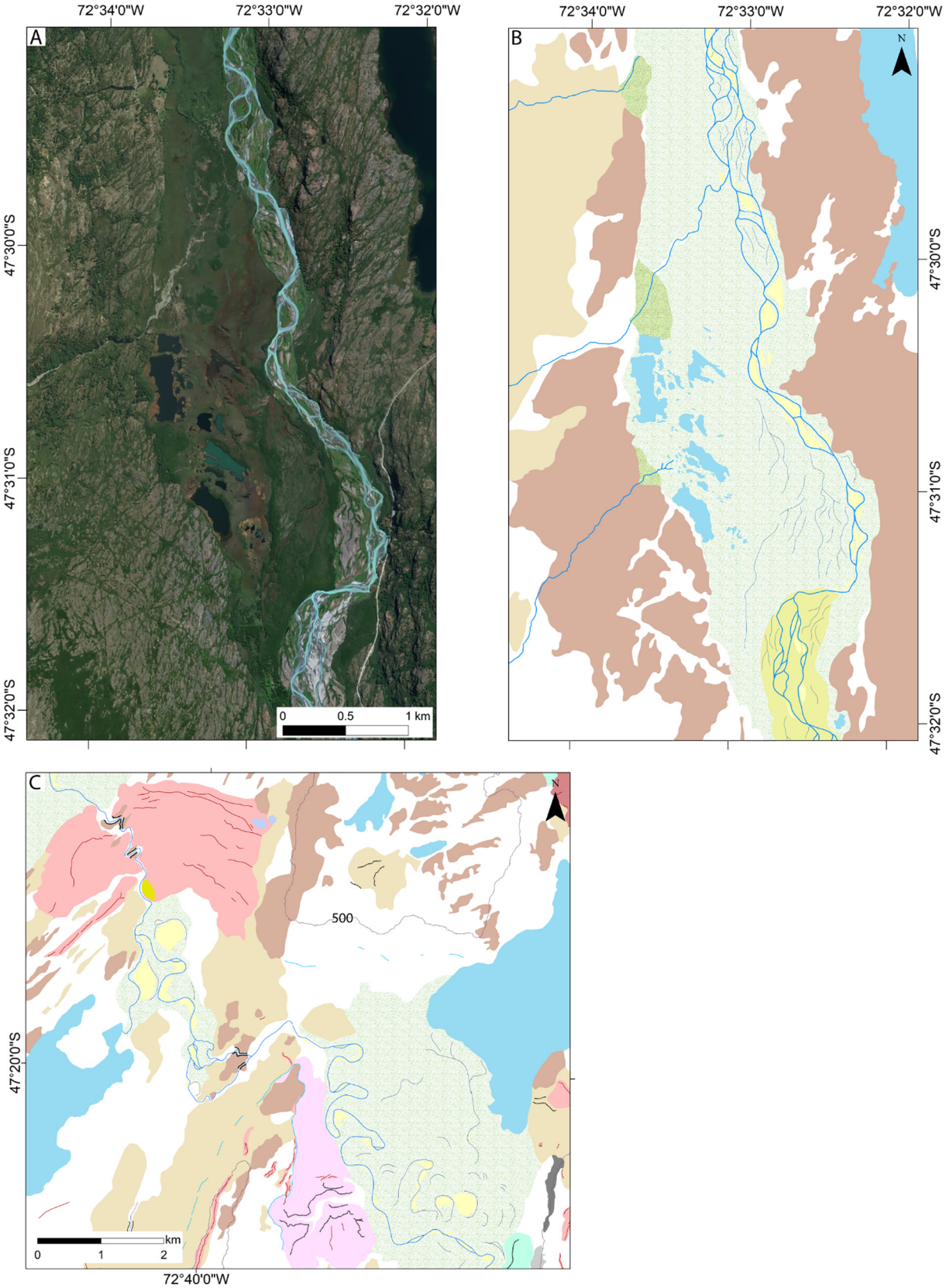

Fig. 15. (A) Satellite image (Digital Globe Esri™) of the Upper Salto valley floor. (B) Mapped landforms in the Salto valley floor, showing the braided Río Salto, channels bars, and pittedlakes. (C) Mapped landforms in the northern Salto valley. Landform colours reflect those in Fig. 2, excluding the pale green speckled polygon which here represents the valley floor floodplain.

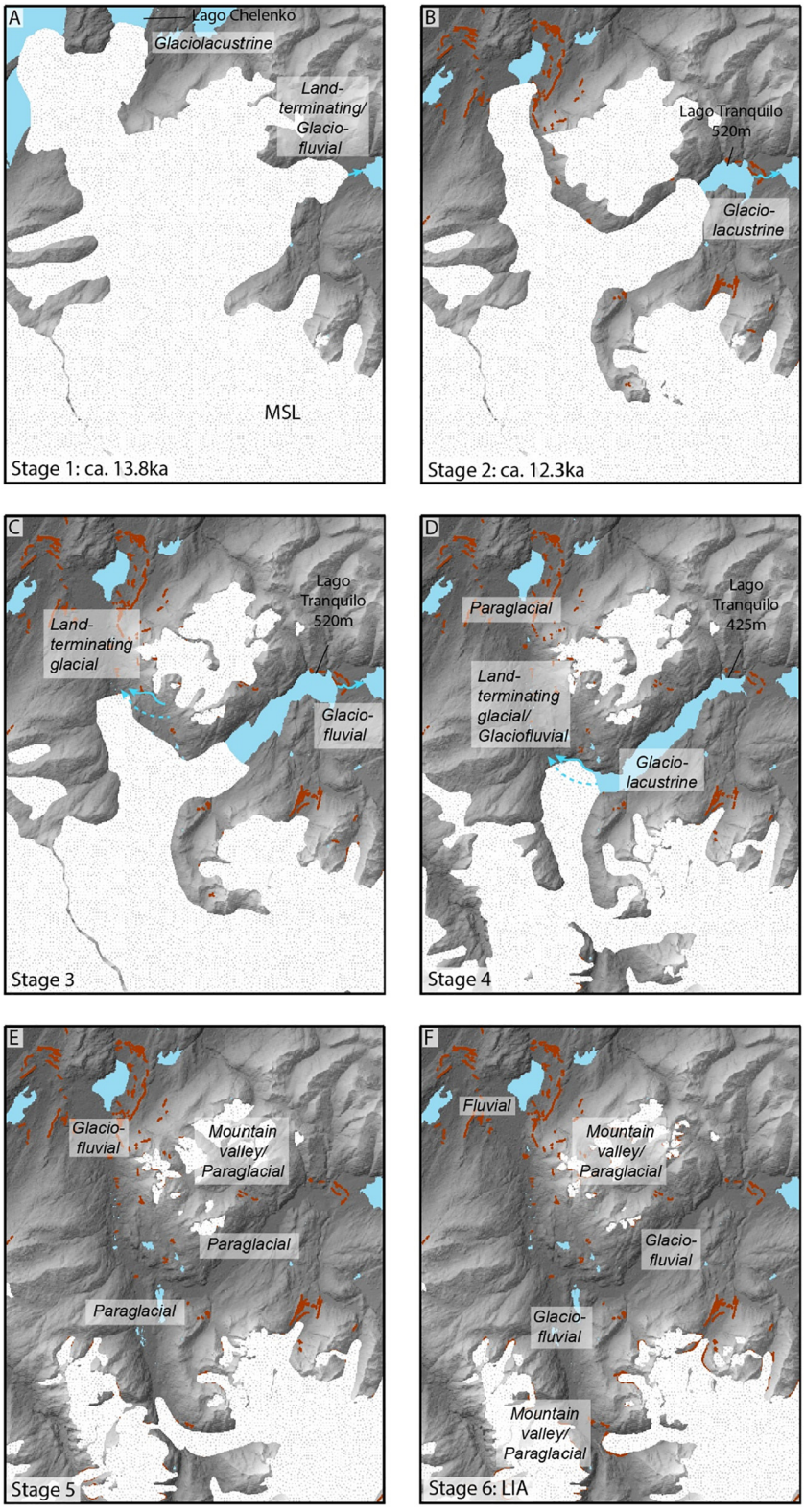

Fig. 16. Glacier, palaeolake and landsystem evolution model of the deglaciation of the northern Monte San Lorenzo ice cap highlighting the evolution in landsystems. Blue arrows show lake outflow pathways. Dashed blue arrow indicates potential subglacial drainage pathway. Red lines show moraine ridges.

Subaerial and subaqueous moraines, subaqueous fans and constant-altitude palaeoshorelines are all found in conjunction.

Silt and clay rhythmites north of Lago Esmeralda (Figs. 3L1, 13A) are typical of ice-distal glaciolacustrine sediments deposited in proglacial lakes, sourced from underflows from the ice front, accompanied by the periodic deposition of ice rafted debris (Church and Gilbert, 1975; Smith and Ashley, 1985; Palmer et al., 2008; Sugiyama et al., 2016). We interpret those exposed at L1 to have formed in this way, in palaeolake Chelenko following ice recession. Those at L2 likely formed in a short-lived ice-contact proglacial lake following ice recession up the Salto valley, dammed by the large M7 moraine ridge. Coarsening to the top of the section into interbedded sands and a diamicton cap is

suggestive of a minor readvance, however could also be the product of increased meltwater input and sediment capacity during the onset of further ice recession.

5.1.2. Land-terminating glacial landsystem

The main landform components of the Salto valley are the cross-valley terminal moraine ridges (M6–M9). (Fig. 4C–E). Due to their substantial size, sharp-crested form and absence of internal deformation structures, we interpret these as dump moraines, formed at the glacier's terminus by the remobilisation of supraglacial debris by roll, fall or glaciofluvial transport during periods of glacier stillstand (Boulton and Eyles, 1979; Benn and Owen, 2002; Benn and Evans, 2010) as ice receded up the Salto valley. Their association with kame terraces and stratified gravel and sand and diamictic composition (e.g., M8, Fig. 6) indicate significant sediment transport and deposition by meltwater at the glacier margins. RA-C_{40} and RWR-C_{40} covariance clast data at moraine sites throughout the Salto valley (Fig. 3) suggest glaciofluvial input and reworking within the subglacial transport system (Lukas et al., 2013). The shallow bed gradient of the Salto valley provides a setting in which an extensive, gently-sloping glacier would be sensitive to small changes in climate and ELA, leading to the formation of multiple cross valley moraine ridges due to numerous small ice margin fluctuations during overall recession. The lack of cross valley moraines in the Pedregoso valley could be the product of an ice mass less responsive to minor climate fluctuations having now receded into a more steeply-sloping valley (Barr and Lovell, 2014). We interpret M11 and M12 as having formed at minor glacier stillstands during glacier recession. Their location, confined to bedrock plateaus on the valley side, suggest that their formation had an element of topographic control.

Significant meltwater input from the glacier terminus proximal to the moraine ridges and from the surrounding catchment, likely contributed to the partial erosion of the M6–M9 moraine ridges. Increased river flow and migration during ice recession up valley would have been significant and, alongside any glacier lake outburst floods, exploited and widened any opening between the ridge and western valley-side. The valley floor is covered by a floodplain, containing a series of kettle-hole lakes, indicating breakoff of ice from the glacier tongue and subsequent burial by glacial outwash.

The exposure of diamicton at S2 is interpreted as subglacial till (Benn and Evans, 2010) with a combination of homogenised material and stratified sediments deposited by water. The presence of water deposited sands and gravels and lack of widespread deformation suggests water flow at the ice-bed interface and ice-bed decoupling (Eyles et al., 1983; Piotrowski and Tulaczyk, 1999; Phillips et al., 2013, 2018). We interpret the two massive gravel features as burst out and simple clastic dyke fluid escape structures, indicating high levels of subglacial water pressure.

5.1.3. Mountain-valley landsystem

The upland valley landsystem in the study area is characterised by a landform assemblage of cirques, saw-tooth moraines, closely-spaced cross-valley moraines, flutes on the valley floor and talus slopes on the surrounding steep valley-sides; the product of recent deglaciation. The closely-spaced moraine ridges are interpreted as push moraines formed during frequent minor readvances or stillstands (cf. Evans et al., 1999, 2018). The larger saw-tooth terminal moraines formed as a result of a more sustained readvance. As ice opens into a less well constrained valley section, radial crevasses form in the glacier tongue resulting in a saw-toothed shaped ice front and moraine ridges with distinctive tooth and notch pairings upon the push up of glacially-reworked material (Matthews et al., 1979; Burki et al., 2009).

Cirques and headwalls with over-deepenings formed by erosion at the base of the glacier through freeze-thaw weathering and plucking (Hooke, 1991) indicating warm-based ice as well as abundant meltwater (Glasser and Bennett, 2004). Flutes are a product of subglacial sediment deformation, forming ridges running parallel to the direction of ice flow under temperate conditions (Boulton, 1976; Gordon et al., 1992; Benn and Evans, 2010). It is to be expected that flutes and small valley-bottom recessional moraine ridges are most commonly found in areas proximal to present-day ice fronts (Benn, 1995; Evans and Twigg, 2002) due to their poor preservation potential (Benn and Evans, 2010). Closely-spaced moraines superimposed on these subglacial bedforms indicate both numerous oscillations of the frontal ice margin and an exposed valley bed not subsequently covered by debris, both indicative of a 'clean' valley glacier (Eyles, 1979; Benn and Evans, 2010).

Unlike in the lower valleys, the glaciofluvial component to the landsystem has a minor impact, manifesting as only narrow single channels, dissecting the cross-valley and saw-tooth moraines in places. The sediment transport pathway is short, with subglacial material sourced from the headwall and cirque bed, and paraglacial processes creating talus slopes bringing material into the valley bottom from the valley sides. Similar cirque architectures are seen on the Isle of Skye at the Coire Lagan formed during the Younger Dryas (Benn and Evans, 2010), as well as in front of present-day, actively-receding glaciers such as at Maradalsbreen, Norway (Benn et al., 2003) and Charquini Sur, Bolivia (Malecki et al., 2018).

5.1.4. Paraglacial landsystem

The paraglacial landsystem is the product of fluvial, flood and slope based processes reshaping the glaciated landscape and can be broken down into a combination of sediment sources, stores, sinks and transport pathways (Ballantyne, 2002). Recently deglaciated and exposed bedrock and drift-mantled slopes in high-altitude valleys and on the slopes above the present-day Calluqueo glacier terminus provide the sediment source for talus slopes and debris cones on the valley sides following rockfall and slope failure. The former are a product of initially large, and later smaller scale rockfalls as part of progressive bedrock adjustment following deglaciation and debutressing (Wyrwoll, 1977; Ballantyne, 2002). Material is glaciofluvially transported and reworked down into the lowland valleys either directly through the main Pedregoso, Salto and Tranquilo river systems or via valley side gullies. At such gullies material manifests as alluvial fans (Figs. 2, 15) forming a secondary sediment store. Material within the primary river systems, and that subsequently reworked from alluvial fans, is redistributed as floodplain valley-fill deposits. The product of this is a floodplain with a braided river system and associated point bar deposits. Meltwater fed rivers with variable annual and seasonal discharge lead to a dynamic migratory river system, producing braiding and abandoned palaeochannels. A lack of subsequently formed river terraces along the Salto valley suggest a maintained sediment supply and balance between sediment input, transport through and redistribution across the valley. There may be slight positive balance in favour of sediment input to counter incision expected as a product of isostatic uplift.

5.1.5. Glaciofluvial landsystem

Glaciofluvial process operate at the lateral and frontal ice-margins forming kame terraces and outwash plains in the Salto and Tranquilo valleys respectively in conjunction with the land-terminating glacial landsystem, and as part of the paraglacial landsystem following deglaciation as in Section 5.1.4. Glaciofluvial processes dominate the proglacial environment forming braided valley trains in sparsely vegetated, non-cohesive material; a product of high bedloads and fluctuations in glacially fed discharge (Miall, 1992; Marren, 2005). Such a feature is found in the southern reach of the Pedregoso valley at the outflow of Lago Calluqueo a steep gradient of 6 to 7 m km^{-1}, typical of braided systems (Benn and Evans, 2010). In the more gently sloping Salto and Tranquilo valleys (1.5 to 2 m km^{-1}), through to the northern reach of the Salto valley adjacent to Lago Esmeralda, the river transitions from a braided system to an increasingly sinuous main river channel with channel bars, islands and occasional subsidiary channels. Finally

the Rio Salto establishes a meandering fluvial landsystem with point bars, palaeochannels and palaeobars in a wider floodplain (Fig. 15C) (Miall, 1985).

5.2. Spatial and temporal evolution of landsystems

Davies et al. (2018) found that during an ACR readvance, ice sourced from Monte San Lorenzo occupying the northern Salto valley discharged into the ca. 350 m asl Lago Chelenko, and formed the Esmeralda moraines (M1a) at 13.2 ± 0.6 ka (Fig. 16A). The glacier terminus remained in a glaciolacustrine environment likely during the first ca. 1000 years of subsequent recession until drainage of Lago Chelenko at ca. 12.4–11.8 ka (Thorndycraft et al., 2019) (Fig. 16B). At this time the glacier terminus was approximately at the margin of M5. Following lake drainage, the glacier became land-terminating and receded up the Salto valley with periodic stillstands or minor readvances (Fig. 16C). A land-terminating glacial landsystem operated during the Holocene in the Salto valley and then continuing in the Pedregoso valley as ice receded further (Fig. 16C to F). Following the Little Ice Age and the formation of M13 the present-day Calluqueo glacier terminated into Lago Calluqueo in a glaciolacustrine setting, before receding to its present-day, land-terminating position.

Ice occupying the Tranquilo valley, after initially existing in a land-terminating setting and forming the Brown moraines (Fig. 16A), receded west into the newly formed 520 m asl ice-dammed palaeolake Tranquilo, in turn transitioning into a glaciolacustrine landsystem (Fig. 16B and C). Further recession and the resulting opening of the 425 m spillway at the Tranquilo-Salto confluence produced a drainage reversal of palaeolake Tranquilo (Fig. 16C and D) with the Brown moraines outflow pathway abandoned at 520 m asl when lake level fell to 425 m asl. This drainage reversal would therefore have contributed increased meltwater flux as well as likely GLOF drainage events, a hypothesis supported by the Salto moraine boulder bar and incised bedrock reaches (Fig. 15C).

Following final drainage of palaeolake Tranquilo as ice receded out of the Tranquilo valley, ice receded up the Pedregoso valley (Fig. 16D and E). Radiocarbon dated organics at a road cutting at the confluence of the Tranquilo and Pedregoso valleys (Fig. 1) suggests that ice must have receded out of the Tranquilo valley by at least 10.5 ka, a minimum distance of ca. 23 km from the Esmeralda moraines (M1a) in 2700 years, and a minimum recession rate of 8.5 m/yr.

Once ice had receded up the Pedregoso valleys a paraglacial landsystem operated with rock-slope failure forming talus slopes and cones, and the glaciofluvial remobilisation of glaciogenic sediment deposited as alluvial fans and valley floor floodplain (Fig. 16E). It is evident that the well-vegetated and fluvially-entrenched alluvial fans are no longer depositionally active, but formed during the Holocene following ice recession, and as such resemble Holocene fans found elsewhere (Ryder, 1971; Ballantyne, 1991; Beaudoin and King, 1994). Alongside this, there is little evidence for significant active large scale rock-slope failure, with only isolated minor rock falls on the high valley sides. An evident reduction in glacially conditioned sediment release through either exhaustion of sediment or sediment stability being attained, suggests that the paraglacial period in the Salto, Tranquilo and Pedregoso valleys has ended and moved towards a 'non-glacial' state (Ballantyne, 2003). Clearly active remobilisation of drift-mantled slopes in the most recently deglaciated sections of high-altitude mountain valleys and near present-day ice margins, particularly at Calluqueo, suggest that paraglacial processes currently operate in these areas. The high-sinuosity meanders of the lower Salto valley suggest a transitioning to a fluvial landsystem (Fig. 16F).

5.3. Temperate Patagonian glacier systems during Late Quaternary deglaciation

Most landsystem studies of contemporary glaciers come from terrestrial-terminating, and topographically-unconstrained, piedmont glacier and ice-lobe settings (Bentley, 1996; Andersen et al., 1999; Schlüchter et al., 1999; Glasser et al., 2009) so are not appropriate analogues for the type of mountain icefield landsystems encountered in Patagonia. Furthermore, many formerly glaciated valleys in Patagonia are forested and inaccessible. Therefore, the detailed Late Quaternary landsystem of Monte San Lorenzo, afforded by good availability of sections, provides an important new geomorphological dataset to help understand the dynamics of temperate Patagonian glacier response to warming climate. In particular our geomorphological and sedimentological data will be relevant for understanding the smaller ice caps located in the cordillera (72–73°W) to the east of the Patagonian Icefields (e.g., Araos et al., 2018; Sagredo et al., 2018). These smaller ice-caps have important implications for understanding palaeoclimate (Sagredo et al., 2018) given their position in the Andean rain-shadow. Furthermore, they potentially play a role in controlling regional drainage as demonstrated in the Baker valley through the separation of Monte San Lorenzo and NPI ice (Thorndycraft et al., 2019).

Our sediment-landform data from Monte San Lorenzo demonstrate that the regional glacial geomorphology conforms to the concept of a mountain icefield landsystem (Benn and Evans, 2010). The diverse topography and climatic settings of Monte San Lorenzo result in a broad landsystem encompassing elements of multiple smaller-scale landsystems. Benn et al. (2003) discuss the spatial and temporal changes in glacial landsystems at the Ben Ohau Range in New Zealand, citing long term climate change as the key driver of spatial and temporal landsystem evolution. Similarly, in central Patagonia, atmospheric warming at the end of the ACR caused regional ice recession, and the subsequent drainage of Lago Chelenko to the Pacific (Thorndycraft et al., 2019) and Lago Tranquilo into the Salto valley, changing the terminal ice environment from lacustrine to terrestrial. The glaciolacustrine dynamics of Lago Tranquilo, and in particular the drainage reversal, highlight the important role of topography in local to regional scale landscape change. Across Patagonia, Thorndycraft et al. (2019) hypothesise that although the broad pattern of ice recession may be similar, driven by Southern Hemisphere palaeoclimate, the timing of palaeolake drainage events is diachronous due to regional topographic settings.

Understanding the spatial and temporal glaciolacustrine dynamics of Patagonian glaciers provides insights for the interpretation of the Late Quaternary landform record. As an illustrative example from this study, the only fluvial terraces in the study area are at the upstream end of the former 425 m asl Lago Tranquilo lake level. Repeat satellite-derived valley floor DEMs from the Cachet II ice-dammed lake (Colonia valley, NPI) provide a modern analogue that demonstrates valley floor incision and upstream enlargement of the lake during successive lake drainage-refill events (Jacquet et al., 2017). Using this analogue for palaeolake Tranquilo, we interpret that the formation of the Tranquilo terraces were caused by base-level fall from palaeolake drainage rather than regional tectonic (Guillaume et al., 2013) or isostatic uplift (Thorndycraft et al., 2019). Our study therefore demonstrates the need for a detailed, holistic approach to the elucidation of glacier, lakes and topographic interactions.

6. Summary and conclusions

We have used detailed geomorphological mapping and sedimentology to describe the landforms and sediments found in valleys directly north of Monte San Lorenzo in Chilean Patagonia.

- The primary landforms identified in the study area are lateral and terminal moraine ridges, ice-scoured bedrock, cirques and headwalls, flutes, deltas, ice-contact fans, glaciolacustrine deposits, palaeoshorelines, kame terraces and outwash and floodplains. These form ice-marginal, subglacial, glaciolacustrine, glaciofluvial and paraglacial sediment-landform associations, from which we infer a range of glacial and paraglacial processes which led to their formation through the Late Pleistocene and Holocene.

- We have identified 7 new moraine sets and ground-truthed and extended the spatial extent of a further 7 through extensive field mapping. This highlights the limitations of identifying and mapping ice margins from satellite imagery alone and in the absence of high-resolution LiDAR DEMs. It is clear that when possible geomorphological field mapping is required to comprehensively identify ice-marginal glacial landforms.
- Our study reveals glaciolacustrine, land-terminating glacial, mountain valley and paraglacial landsystems within the same valley systems, evolving and transitioning during deglaciation. We identify and constrain for the first time an ice-dammed palaeolake Tranquilo which occupied the Tranquilo valley following recession of ice from the Brown moraines.
- For the period of warming after the ACR we have identified three key controls on sediment-landform associations and landsystem development. Firstly this study region illustrates how climate provides a broad-scale control by both dictating the temperate thermal regime of the glacier and the subglacial bedforms created and by causing overall ice recession. As ice recedes, ice-dammed lake drainage pathways open and frontal margins move to higher elevations, transitioning through landsystems as they do so. Secondly, ice-dammed lakes provide a control on glacier frontal stability and in turn ice-marginal landform formation. Finally, topography operates as a control on both a local scale determining the location of sediment supply, and regionally in combination with ice masses to control the extent and level of ice dammed lakes.

Acknowledgements

Martin, Davies and Thorndycraft undertook fieldwork in November/December 2016 and 2017, funded by London NERC DTP PhD award NE/L002485/1 awarded to Martin. We thank the Quaternary Research Association for additional funding support for fieldwork through the QRA New Research Workers' Award. We thank Dr. Adrian Palmer and two anonymous reviewers for comments which helped improve the quality of the manuscript. We thank all landowners for allowing access to their property during fieldwork.

Appendix A. Supplementary data

Supplementary data related to this article can be found online at https://doi.org/10.1016/j.geomorph.2019.03.007

References

Andersen, B.G., Denton, G.H., Lowell, T.V., 1999. Glacial geomorphologic maps of Llanquihue drift in the area of the southern Lake District, Chile. Geogr. Ann. Ser. A Phys. Geogr. 81, 155–166. https://doi.org/10.1111/1468-0459.00056.

Araos, J.M., Le Roux, J.P., Kaplan, M.R., Spagnolo, M., 2018. Factors controlling alpine glaciations in the Sierra Baguales Mountain Range of southern Patagonia (50° S), inferred from the morphometric analysis of glacial cirques. Andean Geol. 45, 357. https://doi.org/10.5027/andgeoV45n3-2974.

Araya, P.S., Sagredo, E.A., Lowell, T.V., Aravena, J.C., 2014. Glacial geomorphology at the Rio Tranquilo Valley (47° S): reconstruction of the sequence of glacial events since the late-glacial through the Holocene. American Geophysical Union, Fall Meeting 2014.

Ashley, G.M., 2002. Chapter 11 - glaciolacustrine environments. In: Menzies, J. (Ed.), Modern and Past Glacial Environments. Butterworth-Heinemann, Oxford, pp. 335–359 https://doi.org/10.1016/B978-075064226-2/50014-3.

ASTER GDEM Validation Team, 2011. ASTER global digital elevation model version 2 - summary of validation results. NASA Land Processes Distributed Active Archive Center and the Joint Japan-US ASTER Science Team Report https://doi.org/10.1017/CBO9781107415324.004.

Balco, G., Stone, J.O., Lifton, N.A., Dunai, T.J., 2008. A complete and easily accessible means of calculating surface exposure ages or erosion rates from 10Be and 26Al measurements. Quat. Geochronol. 3, 174–195. https://doi.org/10.1016/j.quageo.2007.12.001.

Ballantyne, C.K., 1991. Holocene geomorphic activity in the Scottish Highlands. Scott. Geogr. J. 107, 84–98. https://doi.org/10.1080/14702540802300167.

Ballantyne, C.K., 2002. Paraglacial geomorphology. Quat. Sci. Rev. 21, 1935–2017. https://doi.org/10.1016/S0277-3791(02)00005-7.

Ballantyne, C.K., 2003. Paraglacial landsystems. In: Evans, D.J.A. (Ed.), Glacial Landsystems. Arnold, London, pp. 432–461.

Barr, I.D., Lovell, H., 2014. A review of topographic controls on moraine distribution. Geomorphology 226, 44–64. https://doi.org/10.1016/j.geomorph.2014.07.030.

Beaudoin, A.B., King, R.H., 1994. Holocene palaeoenvironmental record preserved in a paraglacial alluvial fan, Sunwapta Pass, Jasper National Park, Alberta, Canada. Catena 22, 227–248.

Bell, C.M., 2008. Punctuated drainage of an ice-dammed Quaternary lake in southern South America. Geogr. Ann. Ser. A Phys. Geogr. 90, 1–17. https://doi.org/10.1111/j.1468-0459.2008.00330.x.

Bell, C.M., 2009. Quaternary lacustrine braid deltas on Lake General Carrera in southern Chile. Andean Geol. 36, 51–65. https://doi.org/10.5027/andgeoV36n1-a04.

Bendle, J.M., Palmer, A.P., Thorndycraft, V.R., Matthews, I.P., 2017a. High-resolution chronology for deglaciation of the Patagonian Ice Sheet at Lago Buenos Aires (46.5°S) revealed through varve chronology and Bayesian age modelling. Quat. Sci. Rev. 177, 314–339. https://doi.org/10.1016/j.quascirev.2017.10.013.

Bendle, J.M., Thorndycraft, V.R., Palmer, A.P., 2017b. The glacial geomorphology of the Lago Buenos Aires and Lago Pueyrredón ice lobes of central Patagonia. J. Maps 13, 654–673. https://doi.org/10.1080/17445647.2017.1351908.

Benn, D.I., 1989. Controls on sedimentation in a late Devensian ice-dammed lake, Achnasheen, Scotland. Boreas 18, 31–42. https://doi.org/10.1111/j.1502-3885.1989.tb00368.x.

Benn, D.I., 1992. Scottish landform examples 5: the Achnasheen terraces. Scott. Geogr. Mag. 108, 128–131. https://doi.org/10.1080/00369229218736855.

Benn, D.I., 1995. Fabric signature of subglacial till deformation, Breidamerkurjökull, Iceland. Sedimentology 42, 735–747. https://doi.org/10.1111/j.1365-3091.1995.tb00406.x.

Benn, D.I., 2004. Clast morphology. In: Evans, D.J.A., Benn, D.I. (Eds.), A Practical Guide to the Study of Glacial Sediments. Arnold, London, pp. 92–106.

Benn, D.I., Ballantyne, C.K., 1993. The description and representation of particle shape. Earth Surf. Process. Landf. 18, 665–672. https://doi.org/10.1002/esp.3290180709.

Benn, D.I., Evans, D.J.A., 2010. Glaciers and Glaciation. Second edition. Hodder Education, London (743 pp.).

Benn, D.I., Owen, L.A., 2002. Himalayan glacial sedimentary environments: a framework for reconstructing and dating the former extent of glaciers in high mountains. Quat. Int. 97–98, 3–25. https://doi.org/10.1016/S1040-6182(02)00048-4.

Benn, D.I., Kirkbride, M.P., Owen, L.A., Brazier, V., 2003. Glaciated valley landsystems. In: Evans, D.J.A. (Ed.), Glacial Landsystems. Arnold, London, pp. 372–406 https://doi.org/10.4324/9780203784976.

Bentley, M., 1996. The role of lakes in moraine formation, Chilean Lake District. Earth Surf. Process. Landf. 21, 493–507. https://doi.org/10.1002/(SICI)1096-9837(199606)21:6<493::AID-ESP612>3.0.CO;2-D.

Boulton, G.S., 1976. The origin of glacially fluted surfaces - observations and theory. J. Glaciol. 17, 287–309. https://doi.org/10.3189/S0022143000013605.

Boulton, G.S., Eyles, N., 1979. Sedimentation by valley glaciers: a model and genetic classification. Moraines and Varves 33, 11–23.

Bourgois, J., Cisternas, M.E., Braucher, R., Bourlès, D., Frutos, J., 2016. Geomorphic records along the General Carrera (Chile)–Buenos Aires (Argentina) glacial lake (46°–48°S), climate inferences, and glacial rebound for the past 7–9 ka. J. Geol. 124, 27–52. https://doi.org/10.1086/684252.

Brazier, V., Kirkbride, M.P., Gordon, J.E., 1998. Active ice-sheet deglaciation and ice-damned lakes in the northern Cairngorn Mountains, Scotland. Boreas 27, 297–310. https://doi.org/10.1111/j.1502-3885.1998.tb01423.x.

Brynjólfsson, S., 2015. Dynamics and Glacial History of the Drangajökull Ice Cap, Northwest Iceland. Norwegian University of Science and Technology, Trondheim (Doctoral thesis, 233 pp).

Buizert, C., Cuffey, K.M., Severinghaus, J.P., Baggenstos, D., Fudge, T.J., Steig, E.J., Markle, B.R., Winstrup, M., Rhodes, R.H., Brook, E.J., Sowers, T.A., Clow, G.D., Cheng, H., Edwards, R.L., Sigl, M., McConnell, J.R., Taylor, K.C., 2015. The WAIS divide deep ice core WD2014 chronology - part 1: methane synchronization (68–31 ka BP) and the gas age-ice age difference. Clim. Past 11, 153–173. https://doi.org/10.5194/cp-11-153-2015.

Burki, V., Larsen, E., Fredin, O., Margreth, A., 2009. The formation of sawtooth moraine ridges in Bødalen, western Norway. Geomorphology 105, 182–192. https://doi.org/10.1016/j.geomorph.2008.06.016.

Caldenius, C.R.C., 1932. Las glaciaciones cuaternarias en la Patagonia y Tierra del Fuego: una investigación regional, estratigráfica y geocronológica, una comparación con la escala geocronológica sueca. Dirección General de Minas y Geología 14, 1–164.

Carrivick, J.L., Tweed, F.S., 2013. Proglacial lakes: character, behaviour and geological importance. Quat. Sci. Rev. 78, 34–52. https://doi.org/10.1016/j.quascirev.2013.07.028.

Chandler, B.M.P., Lovell, H., Boston, C.M., Lukas, S., Barr, I.D., Benediktsson, Í.Ö., Benn, D.I., Clark, C.D., Darvill, C.M., Evans, D.J.A., Ewertowski, M.W., Loibl, D., Margold, M., Otto, J.C., Roberts, D.H., Stokes, C.R., Storrar, R.D., Stroeven, A.P., 2018. Glacial geomorphological mapping: a review of approaches and frameworks for best practice. Earth Sci. Rev. 185, 806–846. https://doi.org/10.1016/j.earscirev.2018.07.015.

Church, M., Gilbert, R., 1975. Proglacial fluvial and lacustrine environments. Special Publications of SEPM. Glaciofluvial and Glaciolacustrine Sedimentation SP23, pp. 22–100.

Collinson, J.D., 1996. Alluvial sediments. In: Reading, H.G. (Ed.), Sedimentary Environments: Processes, Facies and Stratigraphy, Third edition Blackwell Publishing, Malden, MA (688 pp.).

Curry, A.M., 1999. Paraglacial modification of slope form. Earth Surf. Process. Landf. 24, 1213–1228. https://doi.org/10.1002/(SICI)1096-9837(199912)24:13<1213::AID-ESP32>3.0.CO;2-B.

Curry, A.M., Cleasby, V., Zukowskyj, P., 2006. Paraglacial response of steep, sediment-mantled slopes to post-'Little Ice Age' glacier recession in the central Swiss Alps. J. Quat. Sci. 21, 211–225. https://doi.org/10.1002/jqs.954.

Darvill, C.M., Stokes, C.R., Bentley, M.J., Evans, D.J.A., Lovell, H., 2017. Dynamics of former ice lobes of the southernmost Patagonian Ice Sheet based on a glacial landsystems approach. J. Quat. Sci. 32, 857–876. https://doi.org/10.1002/jqs.2890.

Davies, B.J., Thorndycraft, V.R., Fabel, D., Martin, J.R.V., 2018. Asynchronous glacier dynamics during the Antarctic Cold Reversal in Central Patagonia. Quat. Sci. Rev. 200, 287–312. https://doi.org/10.1016/j.quascirev.2018.09.025.

Direccion Meteologica de Chile, 2001. Estadistica Climatologia Tomo III.

Douglass, D.C., Singer, B.S., Kaplan, M.R., Mickelson, D.M., Caffee, M.W., 2006. Cosmogenic nuclide surface exposure dating of boulders on last-glacial and late-glacial moraines, Lago Buenos Aires, Argentina: interpretive strategies and paleoclimate implications. Quat. Geochronol. 1, 43–58. https://doi.org/10.1016/j.quageo.2006.06.001.

Evans, D.J.A., Benn, D.I., 2004. A Practical Guide to the Study of Glacial Sediments. Arnold, London (266 pp.).

Evans, D., Twigg, D., 2002. The active temperate glacial landsystem: a model based on Breiðamerkurjökull and Fjallsjökull, Iceland. 21, 2143–2177 (doi:Pii S0277-3791(02)00019-7).

Evans, D.J.A., Lemmen, D.S., Rea, B.R., 1999. Glacial landsystems of the southwest Laurentide ice sheet: modern Icelandic analogues. J. Quat. Sci. 14, 673–691. https://doi.org/10.1002/(SICI)1099-1417(199912)14:7<673::AID-JQS467>3.0.CO;2-#.

Evans, D.J.A., Shulmeister, J., Hyatt, O., 2010. Sedimentology of latero-frontal moraines and fans on the west coast of South Island, New Zealand. Quat. Sci. Rev. 29, 3790–3811. https://doi.org/10.1016/j.quascirev.2010.08.019.

Evans, D.J.A., Rother, H., Hyatt, O.M., Shulmeister, J., 2013. The glacial sedimentology and geomorphological evolution of an outwash head/moraine-dammed lake, South Island, New Zealand. Sediment. Geol. 284, 45–75. https://doi.org/10.1016/j.sedgeo.2012.11.005.

Evans, D.J.A., Ewertowski, M., Orton, C., 2017. The glaciated valley landsystem of Morsárjökull, southeast Iceland. J. Maps 13, 909–920. https://doi.org/10.1080/17445647.2017.1401491.

Evans, D.J.A., Ewertowski, M., Orton, C., Graham, D., 2018. The Glacial Geomorphology of the Ice Cap Piedmont Lobe Landsystem of East Mýrdalsjökull, Iceland. Geosciences 8, 194. https://doi.org/10.3390/geosciences8060194.

Eyles, N., 1979. Facies of supraglacial sedimentation on Icelandic and Alpine temperate glaciers. Can. J. Earth Sci. 16, 1341–1361. https://doi.org/10.1139/e79-121.

Eyles, N., Eyles, C., Miall, A.D., 1983. Lithofacies types and vertical profile models: an alternative approach to the description and environmental interpretation diamict sequences. Sedimentology 30, 393–410. https://doi.org/10.1111/j.1365-3091.1983.tb00679.x.

Falaschi, D., Bravo, C., Masiokas, M., Villalba, R., Rivera, A., 2013. First Glacier inventory and recent changes in glacier area in the Monte San Lorenzo Region 47° S, Southern Patagonian Andes, South America. Arct. Antarct. Alp. Res. 45, 19–28. https://doi.org/10.1657/1938-4246-45.1.19.

García, J.L., Kaplan, M.R., Hall, B.L., Schaefer, J.M., Vega, R.M., Schwartz, R., Finkel, R., 2012. Glacier expansion in Southern Patagonia throughout the Antarctic Cold Reversal. Geology 40, 859–862. https://doi.org/10.1130/G33164.1.

García, J.L., Hall, B.L., Kaplan, M.R., Vega, R.M., Strelin, J.A., 2014. Glacial geomorphology of the Torres del Paine region (southern Patagonia): implications for glaciation, deglaciation and paleolake history. Geomorphology 204, 599–616. https://doi.org/10.1016/j.geomorph.2013.08.036.

Gardeweg, M., Sellés, D., 2013. Tephrochronology from Villa Castillo to Lago O'Higgens, Aysenm Chile: new insights on the 6,700 and 3,600 years BP eruptions of Hudson Volvano. Boll. Geofis. Teor. Appl. 54, 155–157.

Gilbert, G.K., 1885. The topographic features of lake shores. USGS Annu. Rep. 5-B, pp. 88–96.

Giles, D.P., Griffiths, J.S., Evans, D.J.A., Murton, J.B., 2017. Chapter 3 Geomorphological framework: glacial and periglacial sediments, structures and landforms. Eng. Geol. Geomorphol. Glaciat. Periglaciated Terrains. Eng. Gr. Work. Party Rep. 28, 59–368. https://doi.org/10.1144/EGSP28.3.

Glasser, N.F., Bennett, M.R., 2004. Glacial erosional landforms: origins and significance for palaeoglaciology. Prog. Phys. Geogr. 28, 43–75. https://doi.org/10.1191/0309133304pp401ra.

Glasser, N.F., Jansson, K.N., 2005. Fast-flowing outlet glaciers of the Last Glacial Maximum Patagonian Icefield. Quat. Res. 63, 206–211. https://doi.org/10.1016/j.yqres.2004.11.002.

Glasser, N.F., Jansson, K., 2008. The Glacial map of southern South America. J. Maps 4, 175–196. https://doi.org/10.4113/jom.2008.1020.

Glasser, N.F., Jansson, K.N., Harrison, S., Rivera, A., 2005. Geomorphological evidence for variations of the North Patagonian Icefield during the Holocene. Geomorphology 71, 263–277. https://doi.org/10.1016/j.geomorph.2005.02.003.

Glasser, N.F., Jansson, K.N., Harrison, S., Kleman, J., 2008. The glacial geomorphology and Pleistocene history of South America between 38°S and 56°S. Quat. Sci. Rev. 27, 365–390. https://doi.org/10.1016/j.quascirev.2007.11.011.

Glasser, N.F., Harrison, S., Jansson, K., 2009. Topographic controls on glacier sediment-landform associations around the temperate North Patagonian Icefield. Quat. Sci. Rev. 28, 2817–2832. https://doi.org/10.1016/j.quascirev.2009.07.011.

Glasser, N.F., Harrison, S., Schnabel, C., Fabel, D., Jansson, K.N., 2012. Younger Dryas and early Holocene age glacier advances in Patagonia. Quat. Sci. Rev. 58, 7–17. https://doi.org/10.1016/j.quascirev.2012.10.011.

Glasser, N.F., Jansson, K.N., Duller, G.A.T., Singarayer, J., Holloway, M., Harrison, S., 2016. Glacial lake drainage in Patagonia (13-8 kyr) and response of the adjacent Pacific Ocean. Sci. Rep. 6, 21064. https://doi.org/10.1038/srep21064.

Gordon, J.E., Brian Whalley, W., Gellatly, A.F., Vere, D.M., 1992. The formation of glacial flutes: Assessment of models with evidence from Lyngsdalen, North Norway. Quat. Sci. Rev. 11, 709–731. https://doi.org/10.1016/0277-3791(92)90079-N.

Greenwood, S., 2007. Formalising an inversion methodology for reconstructing ice-sheet retreat patterns from meltwater channels: application to the British Ice Sheet. J. Quat. Sci. 22, 637–645. https://doi.org/10.1002/jqs.

Guillaume, B., Gautheron, C., Simon-Labric, T., Martinod, J., Roddaz, M., Douville, E., 2013. Dynamic topography control on Patagonian relief evolution as inferred from low temperature thermochronology. Earth Planet. Sci. Lett. 364, 157–167. https://doi.org/10.1016/J.EPSL.2012.12.036.

Hein, A.S., Hulton, N.R.J., Dunai, T.J., Sugden, D.E., Kaplan, M.R., Xu, S., 2010. The chronology of the Last Glacial Maximum and deglacial events in central argentine Patagonia. Quat. Sci. Rev. 29, 1212–1227. https://doi.org/10.1016/j.quascirev.2010.01.020.

Hooke, R., 1991. Positive feedbacks associated with erosion of glacial cirques and overdeepenings. Geol. Soc. Am. Bull. 103, 1104–1108. https://doi.org/10.1130/0016-7606(1991)103<1104:PFAWEO>2.3.CO;2.

Jacquet, J., McCoy, S.W., McGrath, D., Nimick, D.A., Fahey, M., O'kuinghttons, J., Friesen, B.A., Leidich, J., 2017. Hydrologic and geomorphic changes resulting from episodic glacial lake outburst floods: Rio Colonia, Patagonia, Chile. Geophys. Res. Lett. 44, 854–864. https://doi.org/10.1002/2016GL071374.

Johnsen, T.F., Brennand, T.A., 2004. Late-glacial lakes in the Thompson Basin, British Columbia: paleogeography and evolution. Can. J. Earth Sci. 41, 1367–1383. https://doi.org/10.1139/e04-074.

Johnsen, T.F., Brennand, T.A., 2006. The environment in and around ice-dammed lakes in the moderately high relief setting of the southern Canadian Cordillera. Boreas 35, 106–125. https://doi.org/10.1111/j.1502-3885.2006.tb01116.x.

Kaplan, M.R., Strelin, J.A., Schaefer, J.M., Denton, G.H., Finkel, R.C., Schwartz, R., Putnam, A.E., Vandergoes, M.J., Goehring, B.M., Travis, S.G., 2011. In-situ cosmogenic 10Be production rate at Lago Argentino, Patagonia: implications for late-glacial climate chronology. Earth Planet. Sci. Lett. 309, 21–32. https://doi.org/10.1016/j.epsl.2011.06.018.

Lal, D., 1991. Cosmic ray labelling of erosion surfaces: in situ nuclide production rates and erosion models. Earth Planet. Sci. Lett. 104, 424–439. https://doi.org/10.1016/0012-821X(91)90220-C.

Livingstone, S.J., Evans, D.J.A., Cofaigh, C., Hopkins, J., 2010. The Brampton kame belt and Pennine escarpment meltwater channel system (Cumbria, UK): morphology, sedimentology and formation. Proc. Geol. Assoc. 121, 423–443. https://doi.org/10.1016/j.pgeola.2009.10.005.

Longhitano, S.G., 2008. Sedimentary facies and sequence stratigraphy of coarse-grained Gilbert-type deltas within the Pliocene thrust-top Potenza Basin (Southern Apennines, Italy). Sediment. Geol. 210, 87–110. https://doi.org/10.1016/j.sedgeo.2008.07.004.

Lukas, S., Benn, D.I., Boston, C.M., Brook, M., Coray, S., Evans, D.J.A., Graf, A., Kellerer-Pirklbauer, A., Kirkbride, M.P., Krabbendam, M., Lovell, H., Machiedo, M., Mills, S.C., Nye, K., Reinardy, B.T.I., Ross, F.H., Signer, M., 2013. Clast shape analysis and clast transport paths in glacial environments: a critical review of methods and the role of lithology. Earth Sci. Rev. 121, 96–116. https://doi.org/10.1016/j.earscirev.2013.02.005.

Malecki, J., Lovell, H., Ewertowski, W., Górski, Ł., Kurczaba, T., Latos, B., Miara, M., 2018. The glacial landsystem of a tropical glacier: Charquini Sur, Bolivian Andes. Earth Surf. Process. Landf. 43, 2584–2602. https://doi.org/10.1002/esp.4417.

Marren, P.M., 2005. Magnitude and frequency in proglacial rivers: a geomorphological and sedimentological perspective. Earth Sci. Rev. 70, 203–251. https://doi.org/10.1016/j.earscirev.2004.12.002.

Matthews, J.A., Cornish, R., Shakesby, R.A., 1979. "Saw-tooth" moraines in front of Bødalsbreen, Southern Norway. J. Glaciol. 22, 535–546. https://doi.org/10.3189/S0022143000014519.

Mendelova, M., Hein, A.S., McCulloch, R., Davies, B., 2017. The Last Glacial Maximum and deglaciation in central Patagonia, 44°S–49°S. Cuad. Investig. Geográfica 43, 719. https://doi.org/10.18172/cig.3263.

Mercer, J.H., 1976. Glacial history of southernmost South America. Quat. Res. 6, 125–166.

Miall, A.D., 1985. Architectural-element analysis: a new method of facies analysis applied to fluvial deposits. Earth Sci. Rev. 22, 261–308. https://doi.org/10.1016/0012-8252(85)90001-7.

Miall, A.D., 1992. Alluvial deposits. Facies model, response to sea level change. pp. 119–142.

Nimick, D.A., McGrath, D., Mahan, S.A., Friesen, B.A., Leidich, J., 2016. Latest Pleistocene and Holocene glacial events in the Colonia valley, Northern Patagonia Icefield, southern Chile. J. Quat. Sci. 31, 551–564. https://doi.org/10.1002/jqs.2847.

Palmer, A.P., Lowe, J.J., 2017. Dynamic landscape changes in Glen Roy and vicinity, west Highland Scotland, during the Younger Dryas and early Holocene: a synthesis. Proc. Geol. Assoc. 128, 2–25. https://doi.org/10.1016/j.pgeola.2017.01.003.

Palmer, A.P., Rose, J., Lowe, J.J., Walker, M.J.C., 2008. Annually laminated Late Pleistocene sediments from Llangorse Lake, South Wales, UK: a chronology for the pattern of ice wastage. Proc. Geol. Assoc. 119, 245–258. https://doi.org/10.1016/S0016-7878(08)80304-5.

Peacock, J.D., 1986. Alluvial fans and an outwash fan in upper Glen Roy, Lochaber. Scott. J. Geol. 22, 347–366. https://doi.org/10.1144/sjg22030347.

Phillips, E., Lipka, E., van der Meer, J.J.M., 2013. Micromorphological evidence of liquefaction, injection and sediment deposition during basal sliding of glaciers. Quat. Sci. Rev. 81, 114–137. https://doi.org/10.1016/j.quascirev.2013.10.005.

Phillips, E.R., Evans, D.J.A., van der Meer, J.J.M., Lee, J.R., 2018. Microscale evidence of liquefaction and its potential triggers during soft-bed deformation within subglacial traction tills. Quat. Sci. Rev. 181, 123–143. https://doi.org/10.1016/j.quascirev.2017.12.003.

Piotrowski, J.A., Tulaczyk, S., 1999. Subglacial conditions under the last ice sheet in northwest Germany: ice-bed separation and enhanced basal sliding? Quat. Sci. Rev. 18, 737–751. https://doi.org/10.1016/S0277-3791(98)00042-0.

Putnam, A.E., Denton, G.H., Schaefer, J.M., Barrell, D.J.A., Andersen, B.G., Finkel, R.C., Schwartz, R., Doughty, A.M., Kaplan, M.R., Schlüchter, C., 2010. Glacier advance in southern middle-latitudes during the Antarctic Cold Reversal. Nat. Geosci. 3, 700–704. https://doi.org/10.1038/ngeo962.

Ramos, V.A., Niemeyer, H., Skarmeta, J., Muñoz, J., 1982. Magmatic evolution of the Austral Patagonian Andes. Earth Sci. Rev. 18, 411–443. https://doi.org/10.1016/0012-8252(82)90047-2.

Ryder, J.M., 1971. The stratigraphy and morphology of para-glacial alluvial fans in south-central British Columbia. Can. J. Earth Sci. 8, 279–298.

Sagredo, Araya, P.S., Lowell, T.V., Aravena, J.C., Kelly, M.A., Schaefer, J.M., 2018. Trans-Pacific glacial response to the Antarctic Cold Reversal in the southern mid-latitudes. Quat. Sci. Rev. 188, 160–166. https://doi.org/10.1016/j.quascirev.2018.01.011.

Schlüchter, C., Gander, P., Lowell, T.V., Denton, G.H., 1999. Glacially folded outwash near Lago Llanquihue, southern Lake District, Chile. Geogr. Ann. 81, 347–358. https://doi.org/10.1111/1468-0459.00062.

Sissons, J.B., 2017. The lateglacial lakes of Glens Roy, Spean and vicinity (Lochaber district, Scottish Highlands). Proc. Geol. Assoc. 128, 32–41. https://doi.org/10.1016/j.pgeola.2015.12.004.

Smith, N.D., Ashley, G., 1985. Proglacial lacustrine environment. Glacial Sedimentary Environments. Special Publications of SEPM https://doi.org/10.2110/scn.85.02.0135.

Sneed, E.D., Folk, R.L., 1958. Pebbles in the lower Colorado River, Texas a study in particle morphogenesis. J. Geol. 66, 114–150. https://doi.org/10.1086/626490.

Stern, C.R., Moreno, P.I., Sagredo, E., Aravena, J.C., 2016. Holocene tephrochronology around Cochrane (~47°S), southern Chile. Andean Geol. 43, 1–19. https://doi.org/10.5027/andgeoV43n1-a01.

Stone, J.O., 2000. Air pressure and cosmogenic isotope production. J. Geophys. Res. 105, 23753–23759. https://doi.org/10.1029/2000JB900181.

Sugiyama, S., Minowa, M., Sakakibara, D., Skvarca, P., Sawagaki, T., Ohashi, Y., Naito, N., Chikita, K., 2016. Thermal structure of proglacial lakes in Patagonia. J. Geophys. Res. Earth Surf. 121, 2270–2286. https://doi.org/10.1002/2016JF004084.

Thorndycraft, V.R., Bendle, J.M., Benito, G., Davies, B.J., Sancho, C., Palmer, A.P., Fabel, D., Armitage, S., Medealdea, A., Martin, J.R.V., 2019. Glacial lake evolution and Atlantic-Pacific drainage reversals during deglaciation of the Patagonian Ice Sheet. Quat. Sci. Rev. 203, 102–127. https://doi.org/10.1016/J.QUASCIREV.2018.10.036.

Turner, K.J., Fogwill, C.J., McCulloch, R., Sugden, D.E., 2005. Deglaciation of the eastern flank of the North Patagonian Icefield and associated continental-scale lake diversions. Geogr. Ann. Ser. A Phys. Geogr. 87, 363–374. https://doi.org/10.1111/j.0435-3676.2005.00263.x.

Wenzens, G., 2002. The influence of tectonically derived relief and climate on the extent of the last Glaciation east of the Patagonian ice fields (Argentina, Chile). Tectonophysics 345, 329–344. https://doi.org/10.1016/S0040-1951(01)00219-0.

Wyrwoll, K.-H., 1977. Causes of rock-slope failure in a cold area: Labrador-Ungava. Geol. Soc. Am. Rev. Eng. Geol. 3, 59–67.